

REPORT DOCUMENTATION PAGE

AFRL-SR-BL-TR-99-

Public reporting burden for this collection of information is estimated to average 1 hour per response, including the time for gathering and maintaining the data needed, and completing and reviewing the collection of information. Send comments regarding this collection of information, including suggestions for reducing this burden, to Washington Headquarters Services, Directorate for Information Operations and Reports, 1215 Jefferson Davis Highway, Suite 1204, Arlington, VA 22202-4302, and to the Office of Management and Budget, Paperwork Reduction Project (0704-0188), Washington, DC 20503.

0140

1. AGENCY USE ONLY (Leave blank)		2. REPORT DATE 31 May 1999	3. REPORT TYPE AND STATEMENTS Final
4. TITLE AND SUBTITLE Multicolor Lithography for High Efficiency, Low Insertion Loss NLO Polymer Devices			5. FUNDING NUMBERS C - F49620-97-0009
6. AUTHOR(S) Robert V. Mustacich and Ronald Finn			
7. PERFORMING ORGANIZATION NAME(S) AND ADDRESS(ES) RVM Scientific, Inc. 705-A Firestone Road Goleta, CA 93117			8. PERFORMING ORGANIZATION REPORT NUMBER RVMS-CR-99-01
9. SPONSORING / MONITORING AGENCY NAME(S) AND ADDRESS(ES) AFOSR/NL 801 North Randolph Street Room 732 Arlington, VA 22203-1977			10. SPONSORING / MONITORING AGENCY REPORT NUMBER
11. SUPPLEMENTARY NOTES			
12a. DISTRIBUTION / AVAILABILITY STATEMENT <b>DISTRIBUTION STATEMENT A</b> Approved for Public Release Distribution Unlimited			12b. DISTRIBUTION CODE
Advances in using multicolor lithography to define waveguides in NLO polymer thin films are described in this report. These waveguides are defined by the refractive index gradients produced by optically photoprocessing the polymer films. This process, based on the spatial, temporal, and intensity distribution of laser radiation on the film, permits the 3-dimensional control of refractive index gradients within the film, allowing the fabrication of advanced waveguide structures. Experiments were done on three polymer films developed at USC. Measurements were made of the photoprocessing rates in these films and compared to a theory developed for photoprocessing in photoresist films. The thermal stability of photoprocessed films was investigated. Refractive index changes and optical attenuation in the photoprocessed regions were measured using prism coupling and ellipsometry. An optimal film was selected, and waveguide channels were photoprocessed in it through a mask. These channels were subsequently buried using flooding radiation without the mask. The film was then subjected to reactive ion etching over the channels, removing material at the surface. These experiments demonstrated the feasibility of using optical photoprocessing to create waveguide transitions from large waveguides matching optical fibers to small waveguides for minimizing the spacing of modulation electrodes.			
14. SUBJECT TERMS Insertion Loss      Optical Waveguides NLO Polymer Materials      Electro-Optic Devices		15. NUMBER OF PAGES 44	16. PRICE CODE
17. SECURITY CLASSIFICATION OF REPORT UNCLASSIFIED	18. SECURITY CLASSIFICATION OF THIS PAGE UNCLASSIFIED	19. SECURITY CLASSIFICATION OF ABSTRACT UNCLASSIFIED	20. LIMITATION OF ABSTRACT

NSN 7540-01-280-5500

Standard Form 298 (Rev. 2-89)  
Prescribed by ANSI Std. Z39-18  
298-102

19990607 081

DTIC QUALITY INSPECTED 1

## TABLE OF CONTENTS

2.0 INTRODUCTION .....	3
2.1 Absorption Kinetics .....	5
2.2 Transmittance .....	8
2.3 Outline of the Phase II Report .....	11
3.0 DEVELOPMENTS IN MULTICOLOR LITHOGRAPHY .....	11
3.1 Laboratory System .....	11
3.2 Beam Overlap Calculations .....	13
3.2 Preliminary Work .....	17
3.3.1 Prism Coupling .....	17
3.3.2 <i>PUDR19</i> .....	20
3.3.3 <i>APII</i> .....	22
3.3.4 <i>FTC</i> .....	26
3.3.4.1 Basic <i>FTC</i> Data .....	26
3.3.4.1.1 Ellipsometry .....	26
3.3.4.1.2 Refractive Index and Absorbance .....	27
3.3.4.1.3 Attenuation .....	31
3.3.4.1.4 Transmittance .....	33
3.3 Photolithography of Channel Waveguides .....	40

## 2.0 INTRODUCTION

Ultrafast optical modulation using nonlinear optical (NLO) polymers is a highly promising technology for enabling the full potential of fiber optics communications. NLO polymers can be fabricated into a variety of active and passive communication system components. The particular aspect of NLO polymer technology that has been the focus of this project is an investigation of the feasibility of using these materials to create optical waveguides with a strong electrooptic (EO) response that can be linked with other system components, e.g., fibers, semiconductor modulators, etc.

In general, NLO polymers have been used so far in approaching particular separate requirements for system components: a thermally stable, strong EO response; polymer device compatibility with manufacturing processes for integrated circuits and chip bonding; fabrication processes with fine control of low loss buried waveguides; low-cost, low-loss interconnects to optical fibers, and effective integration of large bandwidth drive electrodes with semiconductor devices. In this project, RVM Scientific (RVMS) has been working to develop a more unified fabrication approach that combines new, strongly optically active, thermodynamically stable EO polymers with processing that enables the development of modulation components coupled with low-loss interconnects with fibers. This work has been done with the subcontracted support of the University of Southern California (USC) through the laboratories of Dr. Larry Dalton and Dr. William Steier.

More specifically, this research is directed toward fabricating optical waveguides in single optical polymer films that provide low-loss interfaces with optical fibers, either to semiconductor modulators or to modulation subsystems within the optical polymers themselves. So far, developing waveguides has involved trade-offs among the requirements for mode size, single mode support, refractive index gradients, mode penetration of the cladding, and losses. For example, approaches using three-layer film devices entail problems such as processing complexities and residual film stresses. Single-film devices, on the other hand, have to accommodate mode size and mode shape mismatches occurring between different components. This last problem is especially significant in coupling optical fibers, with large mode dimensions, to modulators, which require small mode dimensions for enabling low modulation drive voltages and high-bandwidth (low electrode capacitance) response. The coupling problem is illustrated in Figure 1.

Phase I of this project included initial work on the coupling problem. At USC, stable photoinduced refractive index changes resulting from UV exposure of the dye disperse red 19 (DR19) in a copolyester matrix had been demonstrated. Micropatterning of thin films of copolyester DR19 using this photoprocessing, or "photochemical bleaching", procedure were used for fabrication of waveguides and gratings. In Phase I of this project, the polymer/dye system studied was polyurethane/disperse red 19 (PUDR19). This system displays strong absorption in the visible at 475 nm as well as in the UV, and is transparent above 640 nm.

## OPTICAL COUPLING - DRIVE VOLTAGE TRADEOFF

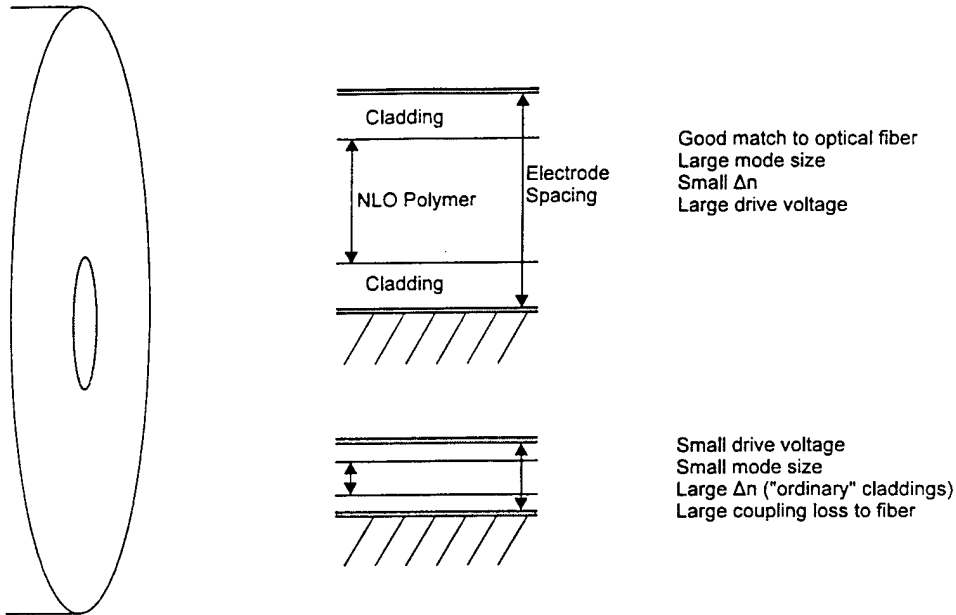


**Figure 1.** Trade-offs between matching mode sizes of single mode fiber and realizing small drive voltages.

Chemical bleaching can be used to fabricate buried channel waveguides in a single film. This procedure is based on the use of *multicolor processing*, which entails at least two steps; one of which uses a mask. It depends on the fact that the penetration of radiation into the sample is a function of the radiation wavelength. Radiation in the absorption band will be absorbed in the upper layers of the film, while out-of-band radiation will penetrate to greater depths because of its greatly reduced absorption.

A cross-section of an idealized buried channel so produced is shown in Figure 5. The buried channel, which can establish single-mode propagation, can be generated by first flooding a film with highly absorbed radiation, creating a low-refractive-index region near the film surface (the effective top cladding in Figure 2), then illuminating the film with more penetrating radiation

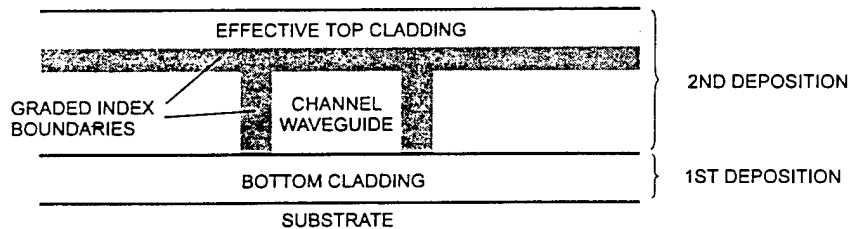


**Figure 2.** Graded index waveguide boundaries resulting from multicolor processing.

through a mask outlining the channel. This second photoprocessing creates low-index regions on the sides of the channeling region, which has been shielded by the mask.

## 2.1 Absorption Kinetics

A mathematical model has been developed (Dill et al, IEEE Trans. Electron Dev. ED-22, 445, July, 1975) for the time-dependent spatial concentration of photoresist components in thin films in response to photoprocessing irradiation. The equations for the time- and depth-dependent intensity and absorber concentration are written in terms of coefficients  $A$ ,  $B$ , and  $C$ , which in turn are expressed in terms of the photoprocessing kinetics of the absorber, specifically:

$$A = \frac{1}{d} \ln \left( \frac{T(\infty)}{T(0)} \right) \quad (1)$$

$$B = -\frac{1}{d} \ln T(\infty) \quad (2)$$

$$C = \frac{A + B}{AI_0 T(0) [1 - T(0)]} \frac{dT(0)}{dt} \quad (3)$$

where  $I_0$  is the incident intensity,  $d$  is the film depth, and  $T(0)$  and  $T(\infty)$  are the film transmittances at the beginning of exposure and at full exposure, respectively. Thus, given a film of known depth and a monochromatic incident beam, the  $A$ ,  $B$ , and  $C$  coefficients can be determined by measuring the transmittance as a function of time. Knowing  $A$ ,  $B$ , and  $C$  for wavelengths in different regimes of an absorption band then enables the design of buried channel waveguides in the film, since refractive index changes are proportional to photochemical changes in NLO polymer dye concentrations. This model was used extensively in the Phase II work.

A simple kinetic model for the absorber destruction and the beam absorption yields the following equations for  $I$  and  $M$  (see Dill's paper):

$$\frac{\partial I(x,t)}{\partial x} = -I(x,t)[AM(x,t) + B] \quad (4)$$

$$\frac{\partial M(x,t)}{\partial t} = -I(x,t)M(x,t)C(I) \quad (5)$$

The initial conditions (before exposure) for  $I$  and  $M$  are

$$M(x,0) = 1 \quad (6)$$

$$I(x,0) = I_0 \exp[-(A+B)x] \quad (7)$$

and the boundary conditions (at the absorber-air interface) are

$$I(0,t) = I_0 \quad (8)$$

$$M(0,t) = \exp[-I_0 C(I)t] \quad (9)$$

where  $I_0$  is the incident radiation intensity.

Note that, in Equation (5) and the second boundary condition, Equation (9),  $C$  has been written as a function of  $I$ , to conform to the results of the transmittance measurements made in this project. In Dill's original paper, the equations were integrated based on the assumption that  $C$  was independent of  $I$ , i.e., was constant. In this work,  $C$  must be evaluated at each value of the depth  $x$ , depending on the local value of  $I$ . This turns out to be only a minor extra step in the integration.

For numerical integration, the coupled first-order partial differential equations for  $M$  and  $I$  can be treated like coupled first-order ordinary differential equations. From the equation for  $M$ ,

$$\frac{\partial [\ln M(x,t)]}{\partial t} = -I(x,t)C \quad (10)$$

which yields

$$\ln[M(x,t)] = - \int_0^t I(x,\tau) C d\tau \quad (11)$$

so that, over a short time interval  $\Delta t$ ,

$$\begin{aligned} \ln \left[ \frac{M(x,t+\Delta t)}{M(x,t)} \right] &= - \int_0^{t+\Delta t} I(x,\tau) C d\tau + \int_0^t I(x,\tau) C d\tau \\ &\cong -I(x,t) C \Delta t \end{aligned} \quad (12)$$

Thus, including the dependence of  $C$  on the local value of  $I$ ,  $M$  may be stepped through  $t$  using

$$M(x,t+\Delta t) = M(x,t) \exp[-I(x,t) C(I) \Delta t] \quad (13)$$

Similarly, from the equation for  $I$ ,

$$\ln \left[ \frac{I(x+\Delta x,t)}{I(x,t)} \right] = -[AM(x,t) + B] \Delta x \quad (14)$$

so that

$$I(x+\Delta x,t) = I(x,t) \exp[-[AM(x,t) + B] \Delta x] \quad (15)$$

Several simple computer programs have been written to evaluate  $M$  and  $I$ . For example, using the values of  $A$ ,  $B$ , and  $C$  determined from the transmittance measurements made on FTC, an NLO polymer developed at USC, the profiles for the concentration  $M$  can be calculated as shown in Figure 3.

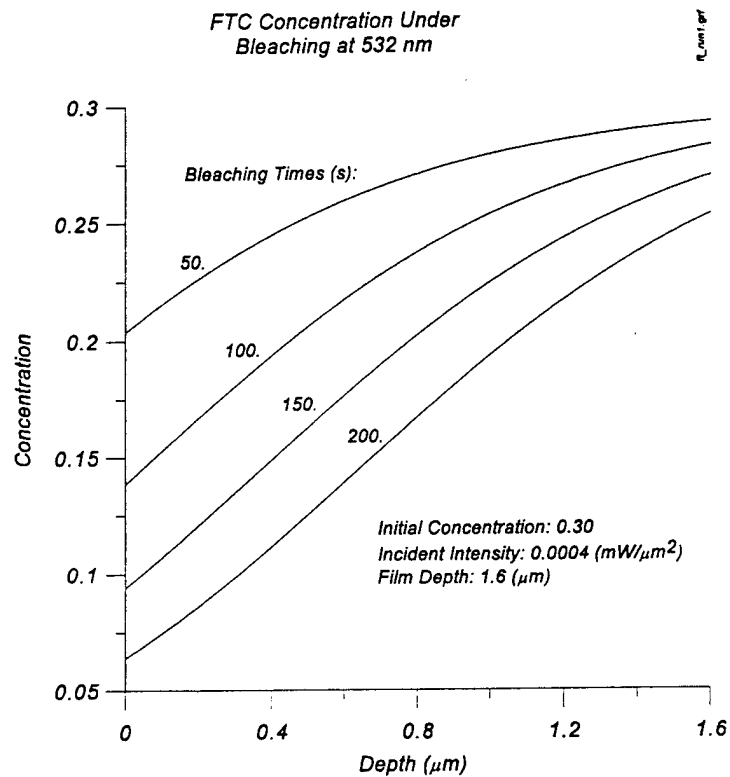


**Figure 3.** Computer Calculations of NLO Polymer Dye Concentration Under Photoprocessing.

## 2.2 Transmittance

The transmittance properties of polymer films are needed to calculate the *ABC* parameters used in the Dill model of film photoprocessing.

The transmittance *T* is calculated from a measurement through a planar medium as shown in Figure 4.

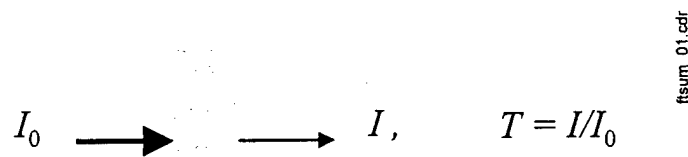


**Figure 4.** Transmittance Through a Planar Medium.

As shown in Figure 4, the transmittance is defined as

$$T = \frac{I}{I_0} \quad (16)$$

where  $I$  is the intensity exiting the medium and  $I_0$  is the input intensity. This definition of transmittance refers to a light/material interaction in a finite layer in an infinite medium; that is, it doesn't include the reflectivities and transmissivities of surfaces the layer might have with other media (including air or vacuum). To properly determine the transmittances of the polymers, these surface effects must be taken into account.

A light beam  $I_i$  incident upon a planar surface between two media results in a reflected beam  $I_r$  and a transmitted beam  $I_t$ , as shown in Figure 5, where  $n_1$  is the refractive index of the medium containing  $I_i$  and  $I_r$ , and  $n_2$  is the refractive index of the medium containing  $I_t$ . It can be shown that, for normal incidence,  $I_r = \mathbf{R}I_i$  and  $I_t = \mathbf{T}I_i$ , where, writing  $n = n_2/n_1$  (Born and Wolf, *Principles of Optics*, 4<sup>th</sup> ed, Pergamon), the reflectivity  $\mathbf{R}$  and the transmissivity  $\mathbf{T}$  are given by:

$$\mathbf{R} = \left( \frac{n - 1}{n + 1} \right)^2, \quad \mathbf{T} = \frac{4n}{(n + 1)^2} \quad (17)$$

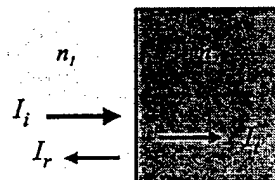
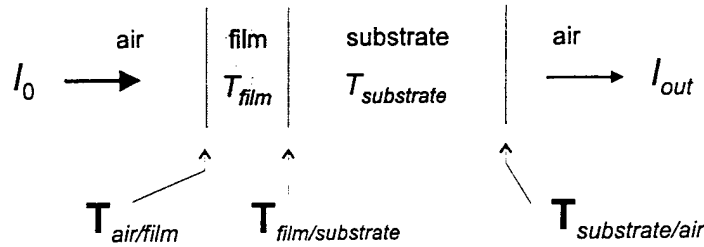


Figure 5. Beam interaction at a surface between two media.

A measurement for the transmittance for a polymer film on a substrate entails measuring the intensity incident upon the film and the intensity emerging from the substrate. To obtain the transmittance of the film, it is necessary to consider three surface transmission coefficients:  $\mathbf{T}_{air/film}$ ,  $\mathbf{T}_{film/substrate}$ , and  $\mathbf{T}_{substrate/air}$ , and the transmittance of the substrate, as shown in Figure 6.



**Figure 6.** Beam interactions traversing a film/substrate system.

From Equations 16 and 17 for  $T$  and  $\mathbf{T}$ , it can be easily shown that measuring the intensities  $I_0$  and  $I_{out}$  for a film/polymer system yields, neglecting the effects of multiple reflections:

$$\frac{I_{out}}{I_0} = T_{film} T_{substrate} \mathbf{T}_{air/film} \mathbf{T}_{film/substrate} \mathbf{T}_{substrate/air} \quad (18)$$

and that measuring  $I_0$  and  $I'_{out}$  for the substrate alone yields:

$$\frac{I'_{out}}{I_0} = T_{substrate} \mathbf{T}_{air/substrate} \mathbf{T}_{substrate/air} \quad (19)$$

From Equation 17 for  $\mathbf{T}$ , it can be seen that, for any two media 1 and 2,  $\mathbf{T}(1 \rightarrow 2) = \mathbf{T}(2 \rightarrow 1)$ ; hence  $\mathbf{T}_{air/substrate} = \mathbf{T}_{substrate/air}$ . Thus  $T_{film}$  is given by

$$T_{film} = \frac{I_{out}}{I'_{out}} \frac{\mathbf{T}_{air/substrate}}{\mathbf{T}_{film/substrate} \mathbf{T}_{air/film}} \quad (20)$$

Since  $n_{film} \approx 1.60$  for most dye/polymer films,  $n_{air} \approx 1.00$ , and assuming that the substrate is BK7 glass ( $n \approx 1.52$ ), the  $\mathbf{T}$ 's may be readily calculated, yielding:

$$\frac{\mathbf{T}_{air/substrate}}{\mathbf{T}_{film/substrate} \mathbf{T}_{air/film}} \approx 1.012 \quad (21)$$

Thus, within experimental error, this quantity may be simply set equal to unity.

## 2.3 Outline of the Phase II Report

Much of the Phase I work was devoted to obtaining  $A$ ,  $B$ , and  $C$  in PUDR19 films at several laser wavelengths. PUDR19 was one of three systems that were examined as part of Phase II of this project, and its photoprocessing kinetics will also be discussed further in the description of the Phase II work.

Section 3 of this Report includes background material for the principal part of the Phase II work: a description of the laser lithography system developed at RVMS, the mechanics of photoprocessing with laser beams, the details of transmittance/absorbance calculations, and a discussion of the selection of the FTC dye/PMMA host system as optimum among the three such systems studied. One critical determination made from these measurements is the fact that the  $C$  parameter is a function of intensity as well as wavelength for at least two dye/polymer systems. Next, there is a discussion of the calculations and measurements made toward developing buried optical channel waveguides in FTC.

Section 4 of this Report includes a discussion of the photoprocessing of channel waveguides in FTC. Measurements of guided-wave attenuation in these channels are described. Two-stage photoprocessing was used to generate buried waveguides, which were etched to demonstrate the feasibility of minimizing modulator dimensions over them.

## 3.0 DEVELOPMENTS IN MULTICOLOR LITHOGRAPHY

### 3.1 Laboratory System

A list of the more significant hardware components of the laboratory system is given in Table 1. It should be noted that the first two items in this list are high-powered visible lasers, which are used for, among other things, photoprocessing the films. Typically, the dyes used in dye/polymer films absorb strongly in the blue region of the spectrum. The dyes are transparent in the infrared; hence waveguides can be developed at 1300 nm, the wavelength selected for this Project.

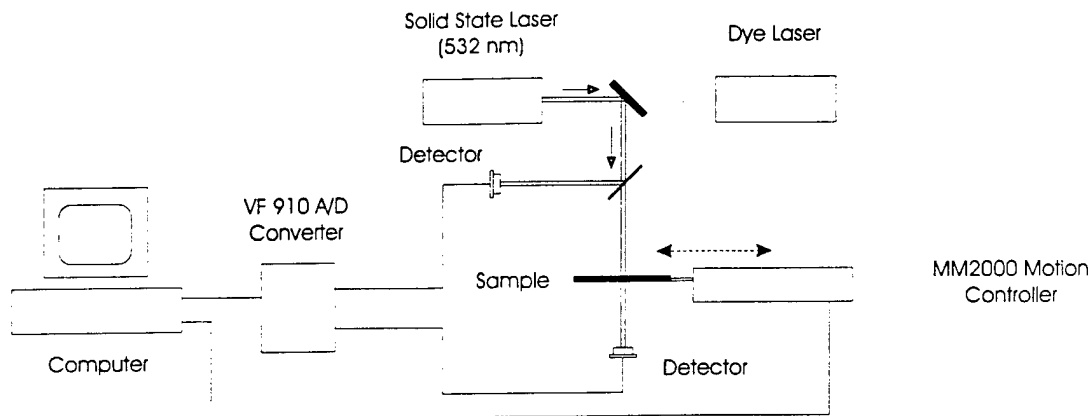
Component	Description	Vendor
Millenia II Diode Pumped CW Visible Laser	Produces up to 2 W CW laser power at 532 nm.	Spectra-Physics
Model 375B Dye Laser	Produces over a hundred mW of CW laser power, which can be tuned over a broad spectral range in the visible region, depending on the dye used.	Spectra-Physics

MotionMaster 2000 Advanced Motion Controller	XYZ translation stage, capable of translation in 2.5 $\mu\text{m}$ steps.	Newport
Model 0108W Laser Profiler	Produces an XY cross section of a laser beam	Photon
VF910 A/D Converter	Analog/Digital converter.	Real Time Devices
Model 310 Laser Power Detector	Measures laser power over a wide dynamic and spectral range	Gentec

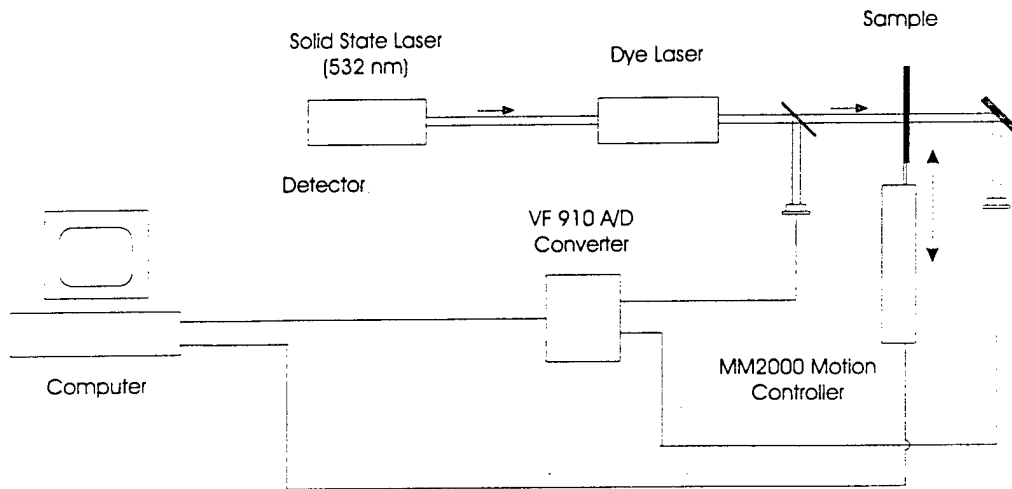
Table 1. Principal System Hardware Components.

In addition to these components, the laboratory is also provided routine instrumentation and supplies such as smaller (HeNe, semiconductor) lasers, photodiode detectors, an optical table, and optical elements (lenses, beamsplitters, compensators, polarizers, holders, positioners, etc.).

Two configurations of the system are outlined in Figure 7. In the first, the 532 nm beam from the Millennia II laser is used as the source beam.; in the second, it is used to pump the dye laser. In each, the beam is steered to the sample polymer film, using mirrors to fold the beam, if necessary. A beamsplitter deflects part of the beam to a detector, usually a photodiode. The MM2000 Motion Controller can be used to maneuver the sample under the beam. Another detector behind the sample captures that part of the beam not absorbed by the sample. These arrangements can be use to measure transmittance and absorbance, perform photoprocessing, etc. If photoprocessing is being performed, the detector behind the sample is usually not used.



(a) Processing Configuration with the Solid State Laser



(a) Processing Configuration with the Dye Laser

Figure 7. Optical Table Configurations.

### 3.2 Beam Overlap Calculations

Photoprocessing will usually be required over an area larger than the cross section of a laser beam. To accomplish a wide area exposure, the beam and the sample must be scanned with respect to each other, as shown in Figure 8. Either the beam can be scanned over the area in a step-and-hold motion that sweeps over the area required, or the sample can be scanned under a stationary beam. This latter approach was used in this Project.

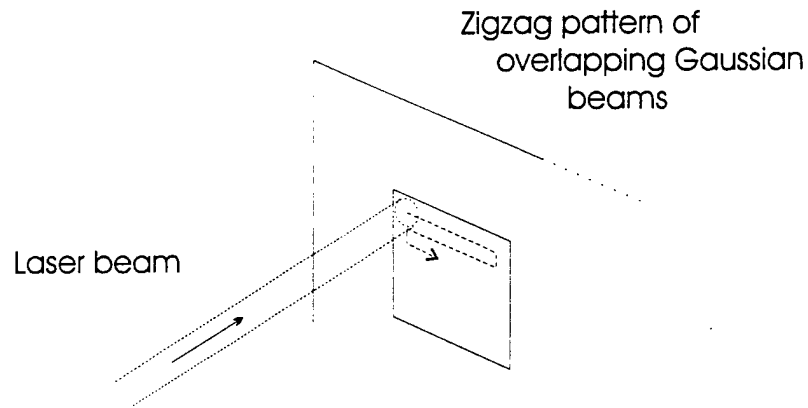


**Figure 8.** Photoprocessing of a Large Sample Area.

Depending upon the absorption, it may be desirable to either expand or focus the beam to adjust its intensity. The Beam Scan is used to check the beam shape after an optical transformation is appropriately 'additive' in its wings; that is, that the beam shape is such that it will yield a predictable intensity when overlapped with itself in a step-and-hold.

A Gaussian beam of monochromatic radiation  $I$  propagating in the  $z$ -direction has a cross-sectional intensity dependence of the form:

$$I = I_0 \exp\left(-\frac{x^2}{2\sigma_x^2} - \frac{y^2}{2\sigma_y^2}\right) \quad (22)$$

where  $I_0$  is the peak intensity and  $\sigma_x, \sigma_y$  are the beamwidth standard deviations. The total power  $P$  in the beam is:

$$\begin{aligned} P &= \int I dA = I_0 \int_{-\infty}^{\infty} dx \exp\left(-\frac{x^2}{2\sigma_x^2}\right) \int_{-\infty}^{\infty} dy \exp\left(-\frac{y^2}{2\sigma_y^2}\right) \\ &= 2\pi I_0 \sigma_x \sigma_y \end{aligned} \quad (23)$$

Thus, for an isolated beam, the peak intensity  $I_0$  is equal to  $P/2\pi\sigma_x\sigma_y$ .

For an overlapping set of beams, the net intensity at a given point is due to the sum of the intensity contributions from all nearby beams; that is, the intensity is given by

$$I = \frac{P}{2\pi\sigma_x\sigma_y} \times f(\Delta_x, \Delta_y; x, y) \quad (24)$$

where  $\Delta x$  and  $\Delta y$  are the  $x$  and  $y$  separations of the beam peaks and  $f(\Delta x, \Delta y; x, y)$  is a factor accounting for all of the contributing beams. A set of plots of  $f$  for a number of values of  $\Delta x$ ,  $\Delta y$ ,  $\sigma_x$ , and  $\sigma_y$  is shown in Figure 9. For a  $\Delta/\sigma$  ratio of  $\leq 2$ , these results show that the overlap of Gaussian beams yields a relatively uniform exposure.

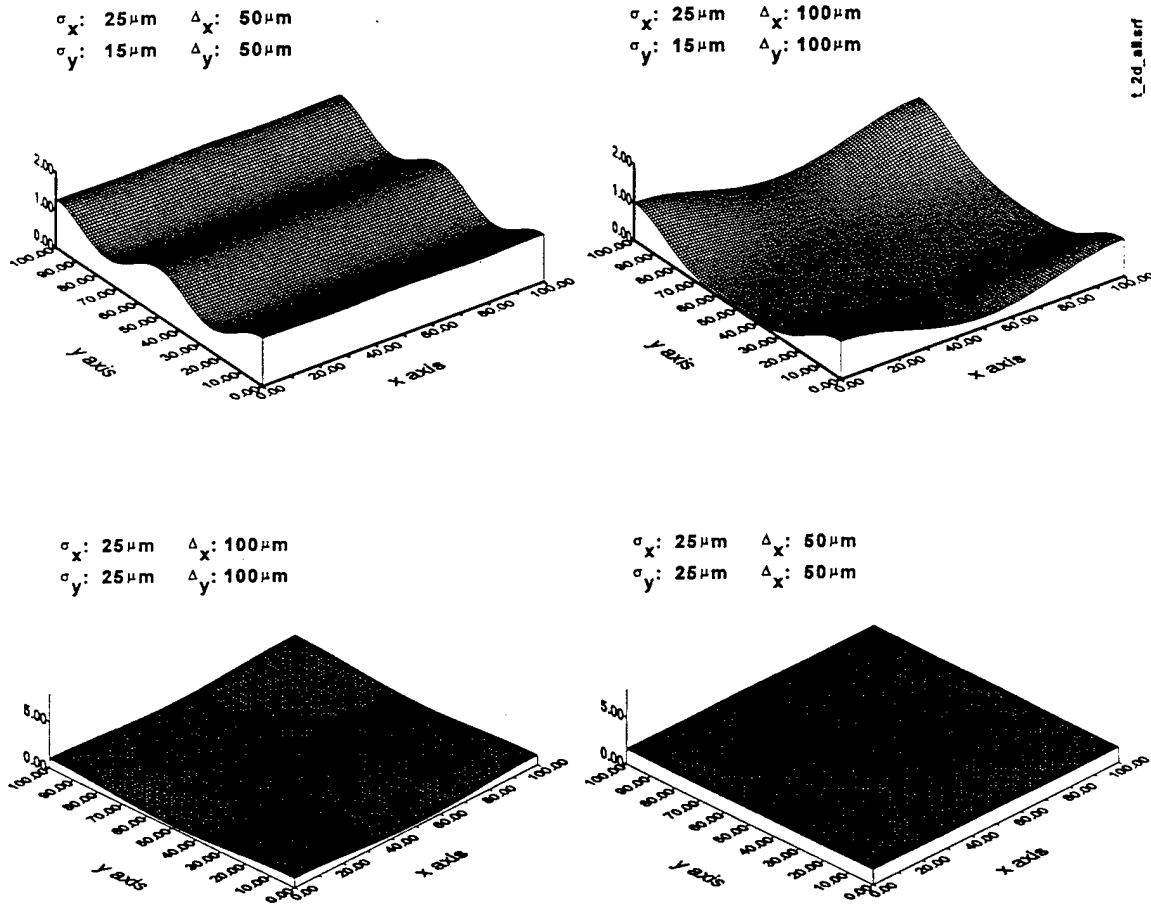
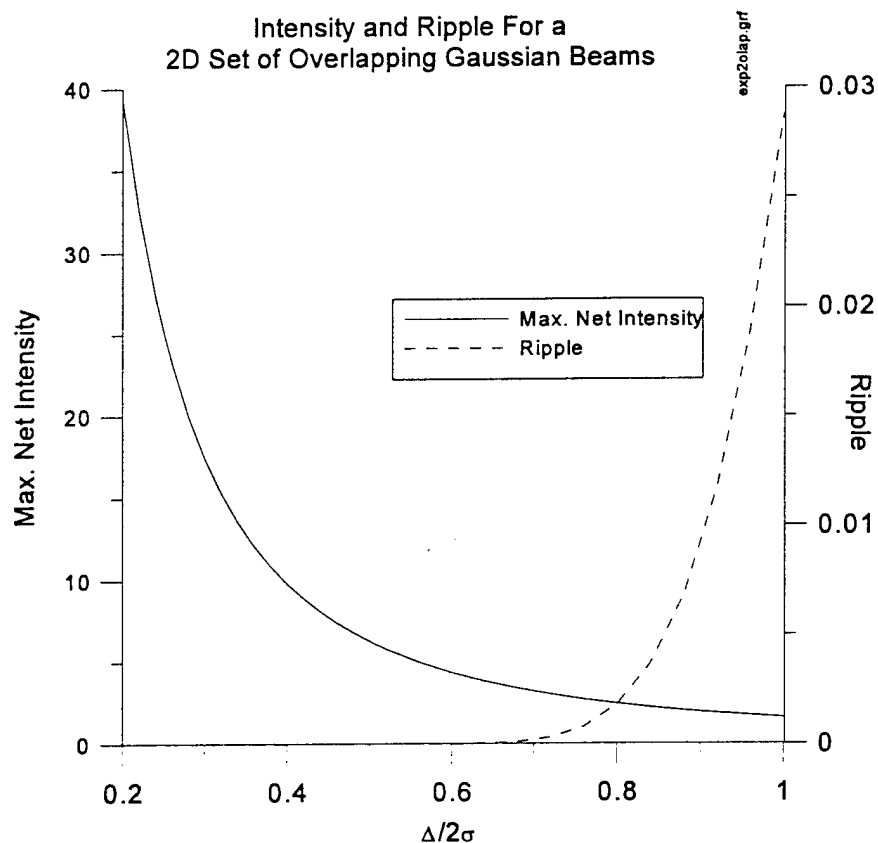


Figure 9. Calculations for the  $f$ -factor for Gaussian beam overlap.

If the beams are close enough together,  $f(x,y) \approx f = (\text{constant})$ , and is independent of the location of the observation point. This can be demonstrated for a set of Gaussian beams of the type shown in Figure 9. The ripple for such calculations can be defined as:

$$ripple = \frac{I_{net}(\text{max}) - I_{net}(\text{min})}{I_{net}(\text{max}) + I_{net}(\text{min})} \quad (25)$$

For the case that the standard deviations  $\sigma_x = \sigma_y = \sigma$  and the step sizes  $\Delta x = \Delta y = \Delta$ , the overlap calculations and the calculations for ripple yield the curves shown in Figure 10. For example, for the particular cases  $\Delta = \sigma/2$  and  $\Delta = \sigma/4$ ,  $f = 6.283$  and  $25.133$ , respectively, with negligible ripple.



**Figure 10.** Maximum net intensity and ripple for a 2D set of overlapping Gaussian beams.

It should be noted that all of the above results only hold for Gaussian beams. Beams with intensity cross-sections differing from a Gaussian profile may require more elaborate calculations

to get the maximum and minimum net intensities. Beam profiles are a function of the source and are sensitive to choice of optics. Beam profiles in our development were monitored and laser profiles and optics were adjusted to maintain Gaussian beam shapes.

## 3.2 Preliminary Work

The development of waveguides in dye/polymer films through photoprocessing first requires detailed measurement and analysis of the dye/polymer system optical properties. In particular, the photoprocessing rates as functions of intensity and wavelength, and the relation between energy deposition (intensity - dwell time product for photoprocessing per unit area) and refractive index must be carefully determined. Using this data, photoprocessing parameters can be calculated for a particular design.

Three dye/polymer film systems have been obtained from USC and studied at RVMS:

- PUDR19, or Disperse Red 19, covalently attached to a polyurethane host.
- APII, also called JT, covalently attached to a polyurethane host.
- FTC, also called FTAC, doped in a polymethyl methacrylate (PMMA) host.

Results of measurements on the first two of these will be described in the rest of this section.

Photoprocessing in these systems was studied using time-dependent transmittance measurements for the three systems. Refractive index measurements were made using prism coupling which will be described below. The refractive index can also be measured using ellipsometry, which will be described as part of the discussion of FTC.

### 3.3.1 Prism Coupling

Prism coupling is a technique for coupling optical radiation into and out of waveguides (Tien, Applied Optics 10, 2395 (Nov. 1971)). Frequently, it is used to measure the waveguide thickness and refractive index. It is implemented as shown in Figure 11, in which a prism is placed in close contact with the surface of the film guide, with no more than a thin air gap between the prism and the film surface. A beam of optical radiation is directed at the prism's angled face, which is then refracted down to the prism face in contact with the film, and then reflected back up. The incident and reflected beams form a standing wave, which then couples through the air gap into the film interior.

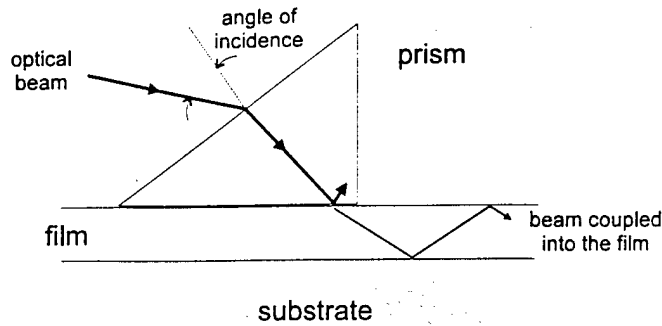


**Figure 11.** Prism Coupling Into a Film Waveguide.

The coupling occurs because the horizontal component of the wave vector in the prism can be matched to the horizontal component of a guided wave vector in the film. This is illustrated in Figure 12, where ‘matching’ refers to the fact that both horizontal components are the same length. Note that the magnitude of a wave vector of light propagating in a medium is  $2n\pi/\lambda$ , where  $n$  is the refractive index of the medium and  $\lambda$  is the wavelength of the light in a vacuum. Note also that the refractive index in the prism must be greater than the refractive index in the film, to insure that the horizontal component of the wave vector in the prism will match the longest possible guided wave vector in the film. A description of wave matching in terms of both ray theory and electromagnetic theory is given in Marcuse, *Theory of Dielectric Optical Waveguides* (Academic Press), where there is also a discussion of the refractive index requirements for waveguiding in a film.

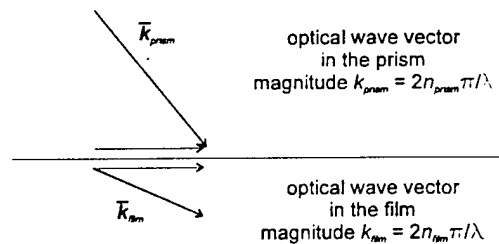


**Figure 12.** Component Matching of Wave Vectors.

In practice, a prism is pressed onto a film surface so that a sufficiently thin air gap is formed near the prism base. Good contact is indicated when, looking into the prism, the contact region looks ‘wet’, indicating that the air gap is less than a wavelength of light thick. Ideally, the ‘wet spot’ should be bigger than the diameter of the optical beam, which is usually sufficiently small so that, for an input prism, the light couples into the film, and doesn’t have room enough to begin coupling back out. Coupling out to detect a beam is accomplished by having a prism facing the

other way pressed down over a beam already in a film.

As pointed out by Marcuse, once light has been coupled into the film, it can propagate (be guided) along the film if its wave vector satisfies certain criteria. As shown in Figure 13, the wave vector magnitude and direction must be such that the optical path length from A to B ( $2\pi \times$  (distance from A to B)/ $\lambda$ ) differs from the optical path length from C to D (which includes the phase shift from two reflections) by a multiple of  $2\pi$ . The phases then reinforce the beam by adding the amplitudes from the separate optical paths, instead of canceling them out. This condition is referred to as a guided *mode*.

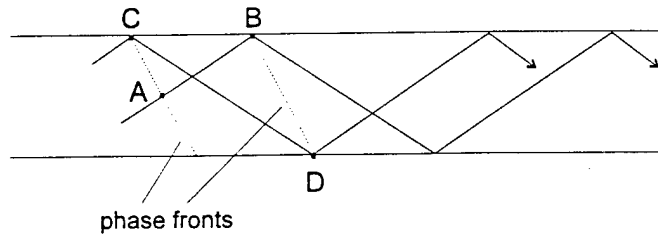


**Figure 13.** Guided Modes Condition.

Because of the conditions imposed on wave propagation in the film, only a finite number of modes are allowed in a film of a given refractive index and thickness. There are two sets of these modes, one set in which the electric vector of the optical field is parallel to the film surface, and another in which the magnetic vector of the optical field is parallel to the film surface. These mode sets can be detected by either using paired input and output single-sided prisms, or, for short guided paths (in cases of high attenuation), by using a double-sided prism (Figure 14). Each mode within a set can be generated by varying the angle of incidence of the beam coming into the input prism. If at least two modes can be detected and their angles of incidence measured, the film thickness and refractive index (at the wavelength used) can be calculated (Kirsch, Applied Optics 20, 2085 (June 1981)).

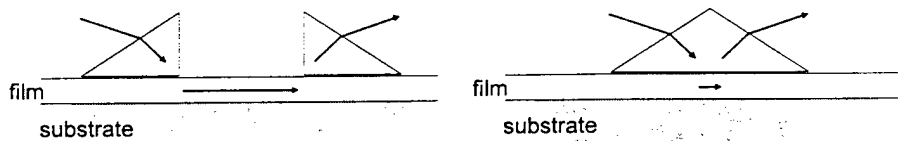


**Figure 14.** Beam Input and Output.

### 3.3.2 PUDR19

PUDR19 is a polyurethane (PU) host doped with the dye Disperse Red 19 (DR19). Experiments were done to photoprocess this film and measure the resulting refractive index changes using prism coupling. The most striking feature of this system is that the photoprocessed areas show birefringence; that is, the refractive index increases in the direction perpendicular to the electric vector of the laser photoprocessing beam, and decreases parallel to it. Data illustrating this effect is shown in Figure 15, in which refractive index measurements at 646 nm using prism coupling (Section 3.3.1) were made at points along a photoprocessed strip (photoprocessed at 532 nm, using the Millennia II laser) with a photoprocessing gradient from one end to the other. The photoprocessing gradient in the energy exposure (intensity - dwell time product) was generated by holding the intensity constant, but increasing the dwell time linearly with displacement along the gradient direction.

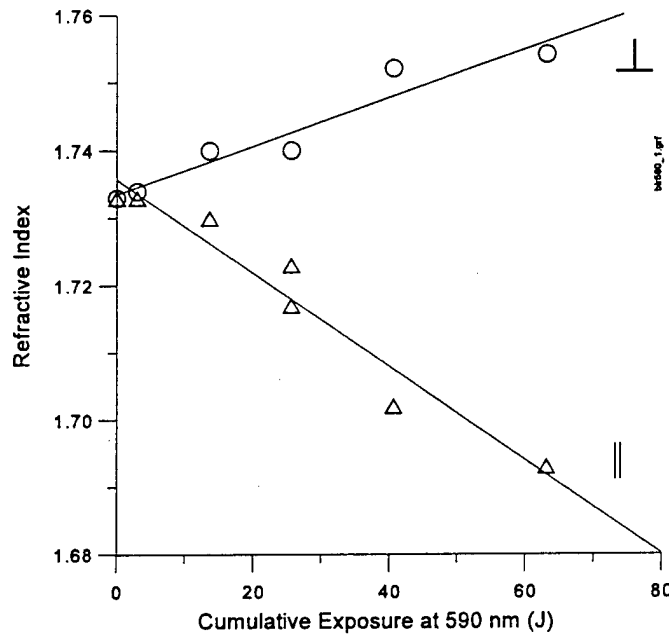
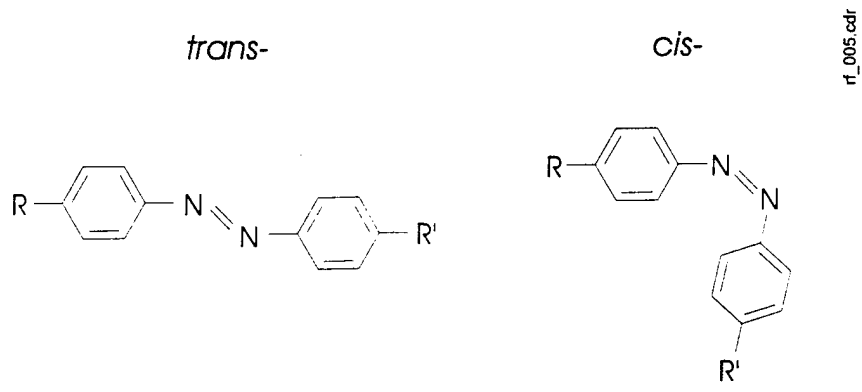


Figure 15. PUDR19 birefringence along a photoprocessed gradient strip.

A model for this photoprocessing is based on the fact that Disperse Red 19 (DR19) is an azo-linked ( $N=N$ ) dye, which has two stereoisomers, *cis*- and *trans*-, as shown in Figure 16, where  $R$  and  $R'$  indicate the remaining parts of the molecule ( $R$ , for example could be the part attaching to the polymer host in the film). At room temperature, most of the dye is in the *trans*-configuration, and in the film, randomly oriented. When photoprocessed with an intense, linearly polarized light beam, some of those *trans*-dye molecules oriented along the  $E$ -field of the light are excited into the *cis*-state. When these excited states relax (back to the *trans*-state), their orientation can change direction, thus some of them become reorientated into directions

perpendicular to the  $E$ -field. The DR19 molecule is more polarizable along its length than perpendicular to it; hence, since the molecules are being driven out of the direction along the  $E$ -field, the film becomes optically anisotropic.



**Figure 16.** Azo dye configurations.

The model of the birefringence resulting from the reorientation of the dye chromophores, rather than their modification or destruction, is corroborated by the fact that the birefringence can be eliminated by heating the film, as shown in Figure 17. These results suggest that heating the film allows the dye chromophores to become randomly orientated again, returning the film to its original state.

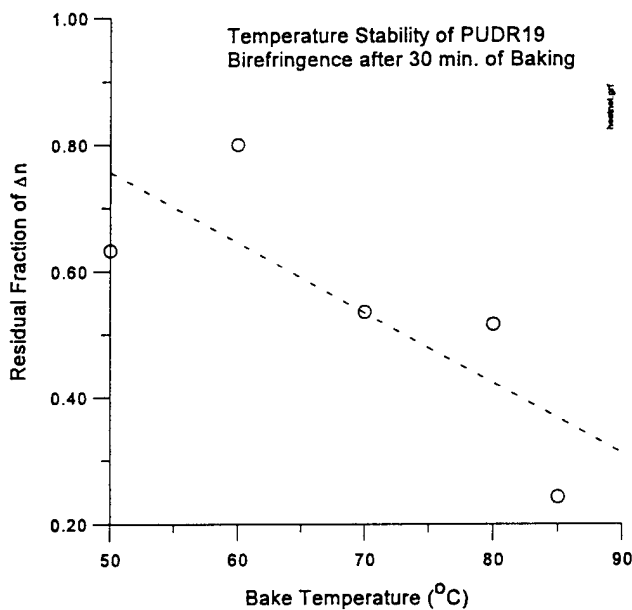


**Figure 17.** Relaxation of birefringence in PUDR19 on heating.

It appears that PUDR19 is an unsatisfactory dye/polymer film system for waveguide generation. The fact that the birefringence entails an increase in the refractive index in two directions creates a difficulty in photoprocessing to achieve lowered refractive indices in regions around a proposed waveguide. While we demonstrated birefringent waveguiding systems using our photoprocessing methods with PUDR19, it is difficult to take full advantage of the multicolor lithography approach because of this birefringence. In addition, the refractive index changes associated with this birefringence are not sufficiently stable thermally.

### 3.3.3 APII

APII, sometimes referred to as JT, is a chromophore covalently attached to PU. A number of photoprocessing and refractive index experiments have been done on this dye/polymer film system provided by USC. Initial photoprocessing and refractive index measurements indicated that, unlike PUDR19, photoprocessed APII displays three important and useful characteristics:

- Thermal stability at 120 °C for at least 10 minutes.
- No birefringence, examined using crossed polarizers.
- Permanent refractive index lowering with photoprocessing.

Absorbance and refractive index measurements were made on an APII film sample on which a linear, photoprocessed gradient region had been generated using the 532 nm light from the Millennia II laser and varying the photoprocessing exposure time. The absorbance was measured along the gradient using 633 nm light from a HeNe laser, and the refractive index was measured using prism-coupled light from a 1300 nm semiconductor laser. These measurements yield absorbance and refractive index variation as a function of energy exposure, both of which are functional relationships needed for designing waveguides. Results are shown in Figure 18.

As discussed for the equations for the Dill model shown on pg. 3, waveguide design and development also require knowledge of the film transmittances at the beginning of exposure and at full exposure. Measurements of transmittance were made by directing a laser beam at a film sample while measuring the power emerging through the substrate as a function of time. The intensity of the beam was estimated from the beam power as described in Equation 23. Graphs of  $T(0)$ ,  $T(\infty)$ , and  $dT(0)/dt$  can be obtained from such measurements as shown in Figure 19. APII shows an initial threshold time before the onset of photoprocessing as shown in Figure 20. Accounting for this, the initial rate of photoprocessing, which is required for the  $C$  parameter, is shown as a function of intensity in Figure 21.

It may be noted in Figure 21 that the initial photoprocessing rate is a function of intensity, an unexpected result. This effect was also seen in FTC, where it will be discussed in regards to waveguide generation.

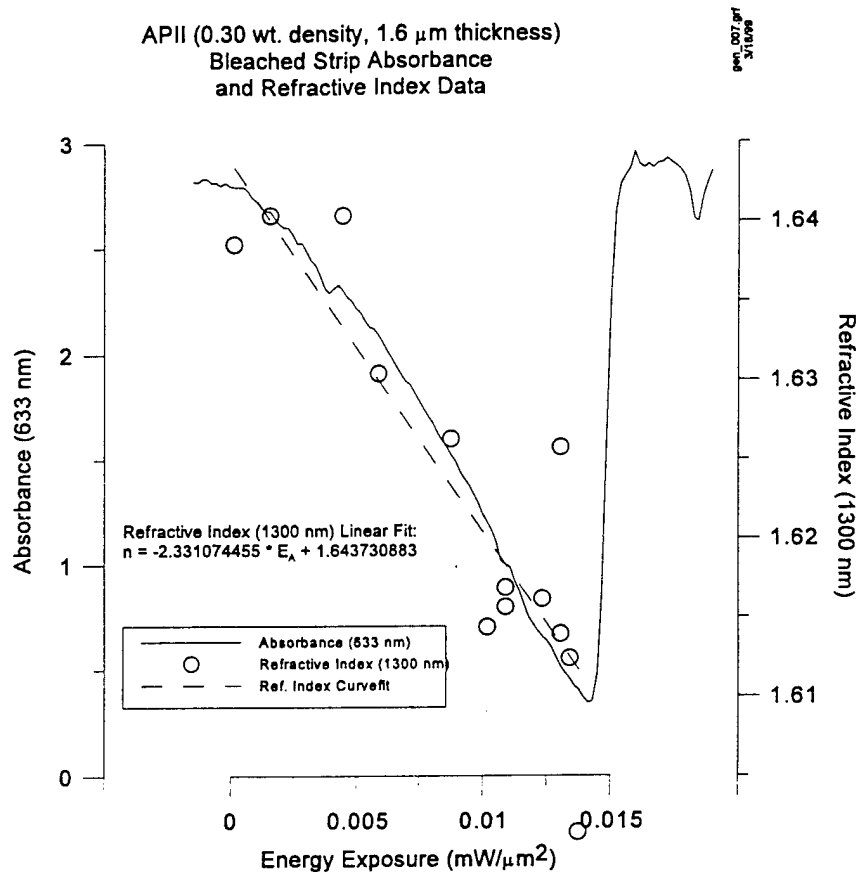


**Figure 18.** Absorbance and Refractive Index Variation Along a Gradient Strip in APII.

The small refractive index changes undergone by APII under photoprocessing make this system attractive for multicolor lithography, since it allows good processing control of small induced refractive index changes ( $\Delta n \approx 0.01$ ) needed for channel waveguides. The refractive index of fully photoprocessed APII remains relatively high as a result of the host PMMA index. Waveguides in APII are irreversible and stable; APII appearing insensitive to low levels of optical irradiation due to environmental light exposure. However, additional work on APII was not undertaken, as FTC was determined at USC to be a preferred system for further waveguide research.

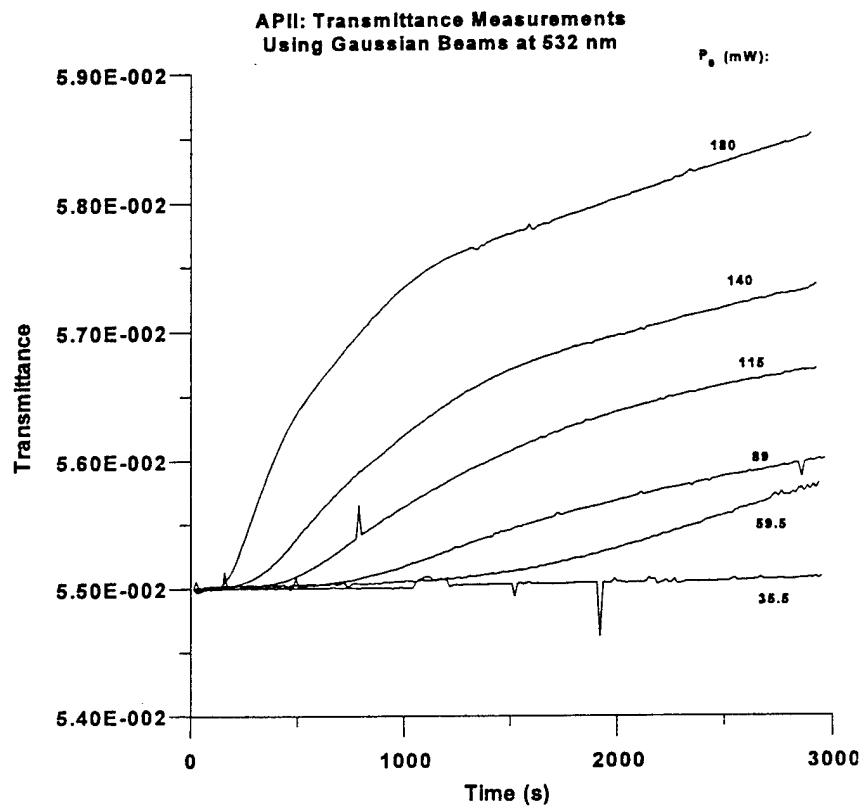


**Figure 19.** Transmittance Measurements in APII under photoprocessing by Gaussian beams.

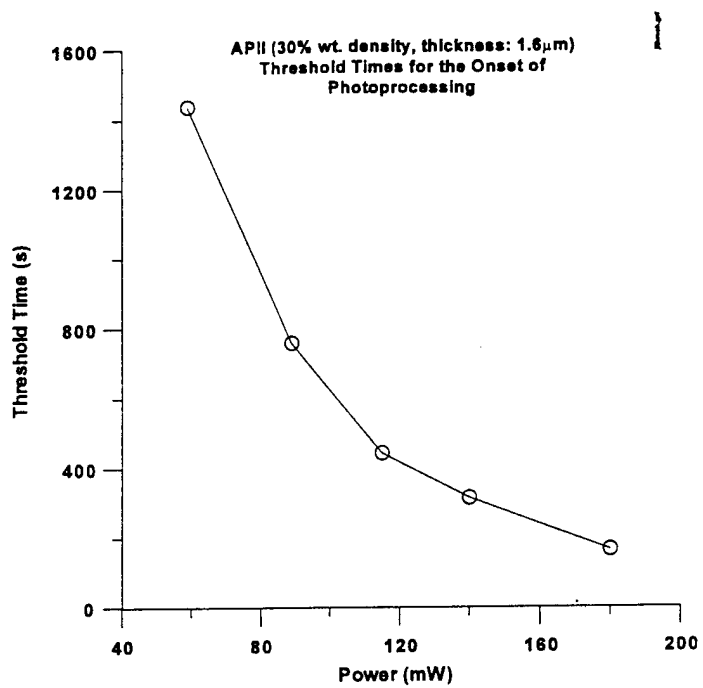


Figure 20. Threshold times for photoprocessing in APII. This threshold is the delay time before the onset of photoprocessing shown in Figure 19.

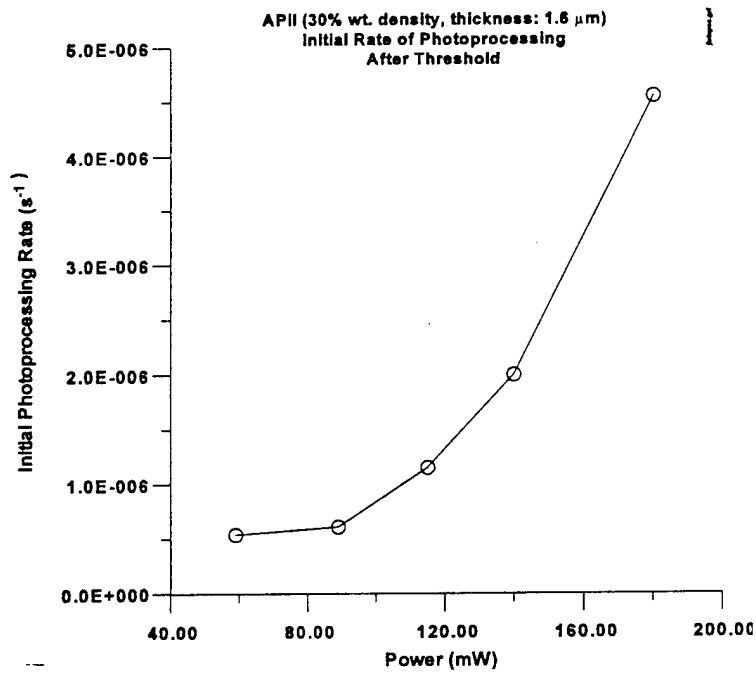


Figure 21. Initial rate of photoprocessing after threshold in APII.

### 3.3.4 FTC

FTC, sometimes referred to as FTAC, is a chromophore doped in a PMMA host.

#### 3.3.4.1 Basic FTC Data

More work was done on FTC than the other systems, and is described in the following sections.

##### 3.3.4.1.1 Ellipsometry

As mentioned on pg 15, the refractive index of thin films can be measured using either prism coupling or optical ellipsometry. Optical ellipsometry refers in general to the measurement of the polarization state of a light wave (Azzam and Bashara, *Ellipsometry and Polarized Light*, North-Holland, 1987). Optical radiation interacting with material media will undergo a change in its polarization state, and these changes can be used to determine the bulk properties of the material.

More specifically, reflection ellipsometry entails shining an optical beam with a known polarization state onto a highly reflecting surface covered (with either a bulk quantity or a thin film) of a material whose refractive index and dispersion are to be determined. These quantities can then be calculated from measuring the how the polarization state of the reflected beam differs from that of the incident beam.

A simplified diagram of the usual experimental setup for these measurements is shown in Figure 22. The polarizer converts randomly polarized light into linearly polarized light, with a polarization along its axis (indicated in the Figure). The compensator has two axes, at right angles to each other. Components of polarization along one axis are retarded in phase with respect to components along the other, converting linearly polarized light into elliptically polarized light. Shining this light into and reflecting it back through the sample material being studied changes its polarization state. The analyzer is simply another polarizer. Its function is to enable the detector to measure the polarization state of the reflected light by measuring its components.

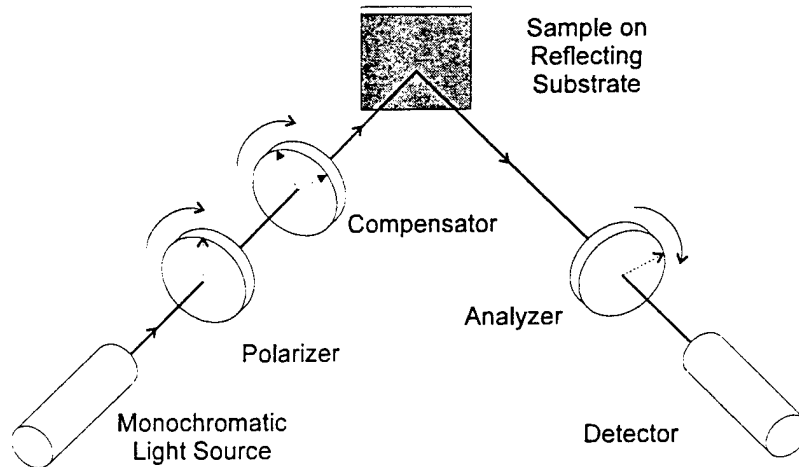


**Figure 22.** Reflection Ellipsometry.

As indicated in Figure 22, the polarizer, compensator, and analyzer can all be separately rotated about the system optical axis. In a typical measurement, all three elements are rotated with respect to each other to give sets of measurements, which usually have to be combined statistically to give a value for an optical parameter such as the refractive index.

#### 3.3.4.1.2 Refractive Index and Absorbance

The refractive index of unphotoprocessed FTC provided by USC is given by the curve in Figure 23. This curve was generated by a set of ellipsometric measurements, and includes a range of infrared wavelengths around  $1.3 \mu\text{m}$ , a design wavelength for waveguides.

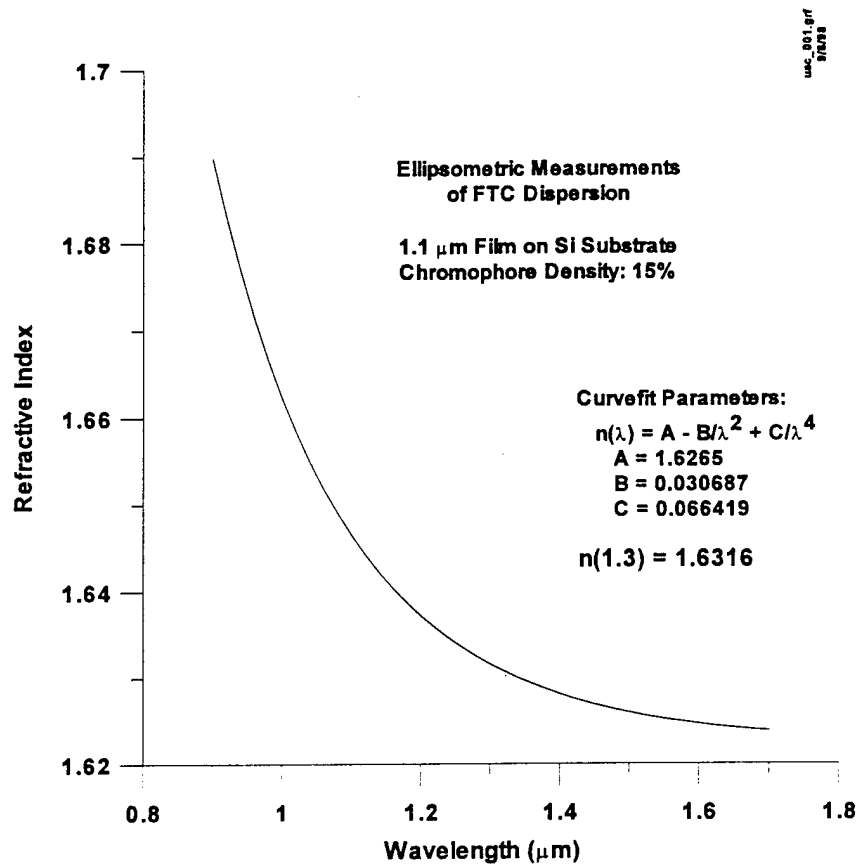


**Figure 23.** Refractive Index of Unphotoprocessed FTC.

A spectrophotometric absorption curve for unphotoprocessed FTC is shown in Figure 24. This curve covers a range of wavelengths from the violet to the near infrared, which would include any possible wavelength used for photoprocessing.

USC Spectrophotometric Measurements of  
FTC Absorbance (15% wt. density)

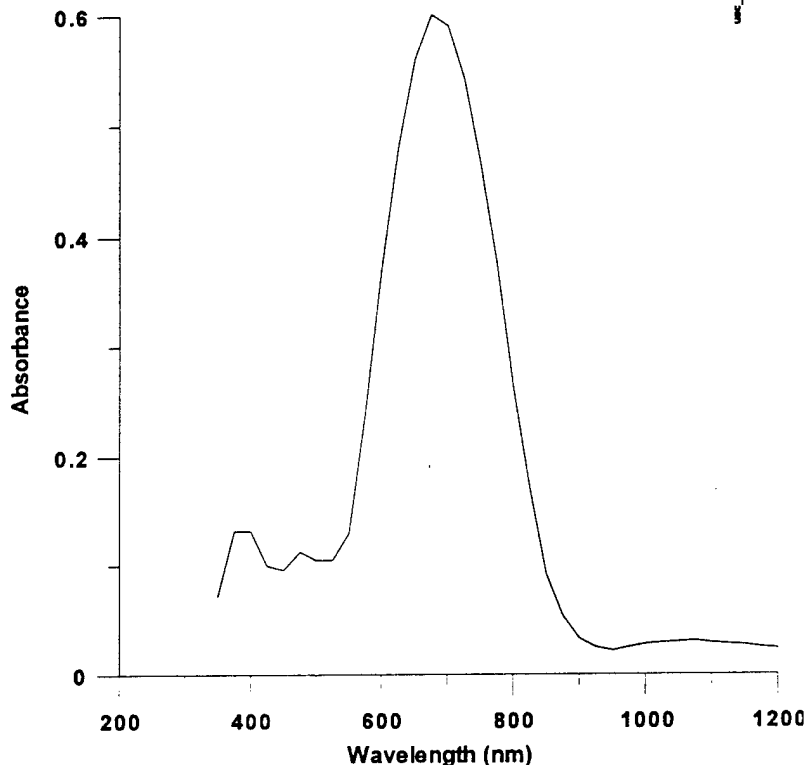
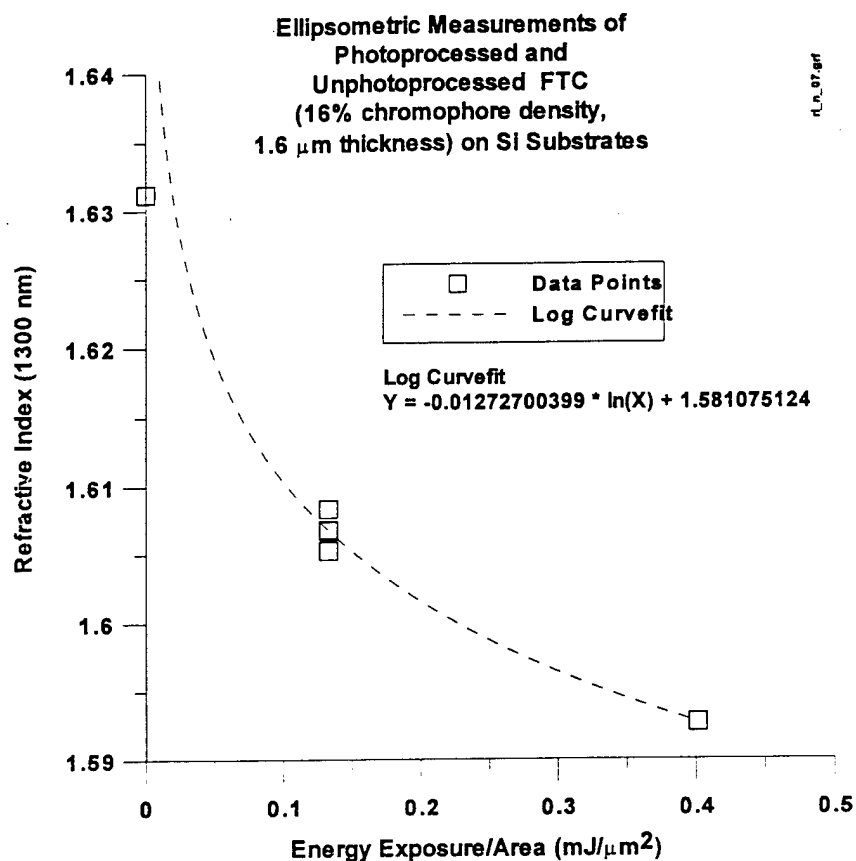


Figure 24. Absorbance of unphotoprocessed FTC.

A considerable effort was made to obtain refractive index data for photoprocessed FTC films, using both prism coupling and ellipsometry. The latter of these two techniques appears to be more accurate. A set of ellipsometer measurements were made on both photoprocessed and unphotoprocessed films on Si substrates. Results for all of these measurements are shown in Figure 25. The data points are plotted against energy exposure/area, which was determined from the photoprocessing laser power (at 532 nm, from the Millennia II laser) dwell times and the beam overlap. All FTC film chromophore concentrations were about 16%. Corrections for the reflectivity of the substrate were estimated as increasing the intensity of the photoprocessing radiation by a factor of about 1.3.



**Figure 25.** Refractive Index Data for FTC at 1300 nm for Photoprocessed and Unphotoprocessed Films on Si.

FTC photoprocesses slowly, with relatively high laser power required. Also, the maximum refractive index is smaller (0.040) than observed with other systems such as the PUDR19 polymer with which this program started. This is important for both process control and precision in producing waveguides. In addition, it renders the FTC films immune to ambient light. Very importantly, it was found that the photoprocessing process in FTC is both stable and irreversible with respect to heating, in contrast to the photoinduced and relatively unstable birefringence effects occurring in PUDR19.

While the photoinduced birefringence in the PUDR19 system relies on a reversible *cis-trans* photoisomerization, the photoinduced refractive index changes in the FTC system appear to be the result of a permanent photochemical change in the dye. This is probably the result of a disruption of the conjugation of the  $\pi$ -electron system of the dye by the photochemistry, which leads to the stability and irreversibility of the refractive index change. This question will be discussed below.

### 3.3.4.1.3 Attenuation

Attenuation measurements were made in FTC using prism coupling as described above in section 3.3.1, and prism coupling using immersion in index matching fluid as discussed in this section. Data for the first of these is shown in Figure 26.

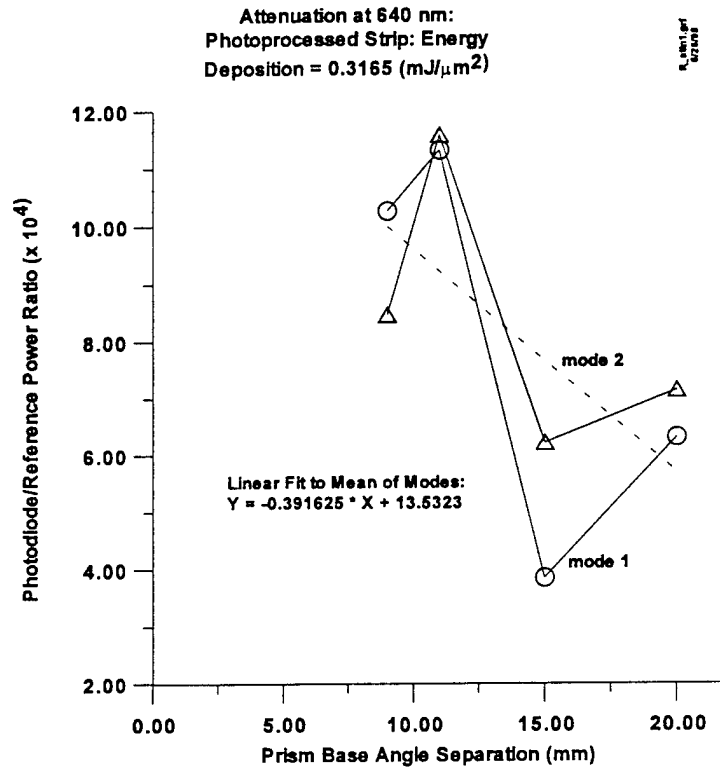


**Figure 26.** Attenuation in FTC for Propagation in Planar Waveguides.

The procedure for absorbance measurements using prism coupling with index matching fluid is illustrated in Figure 27. An input beam is prism-coupled into a film on a substrate, which is slowly lowered into an index-matching fluid. The beam outcouples where the film enters the fluid and is measured by a detector. The power of the beam is thus measured as a function of the distance the beam travels in the film from where it is coupled in, giving a measure of the attenuation.

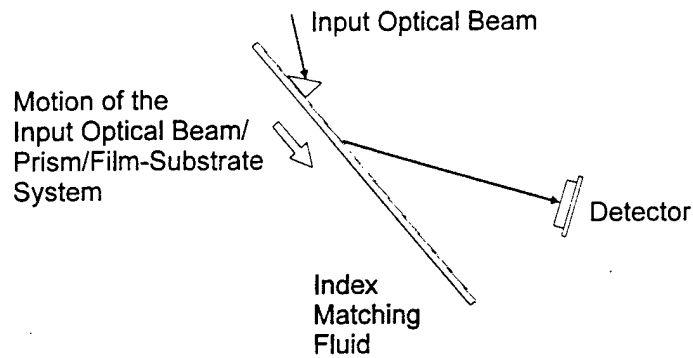


**Figure 27.** Prism Coupling with Index matching Fluid.

A set of measurements using this technique is shown in Figure 28. Here the attenuation is measured as a function of the energy exposure/area used when the film was photoprocessed (as distinct from the energy actually absorbed per area in photoprocessing).

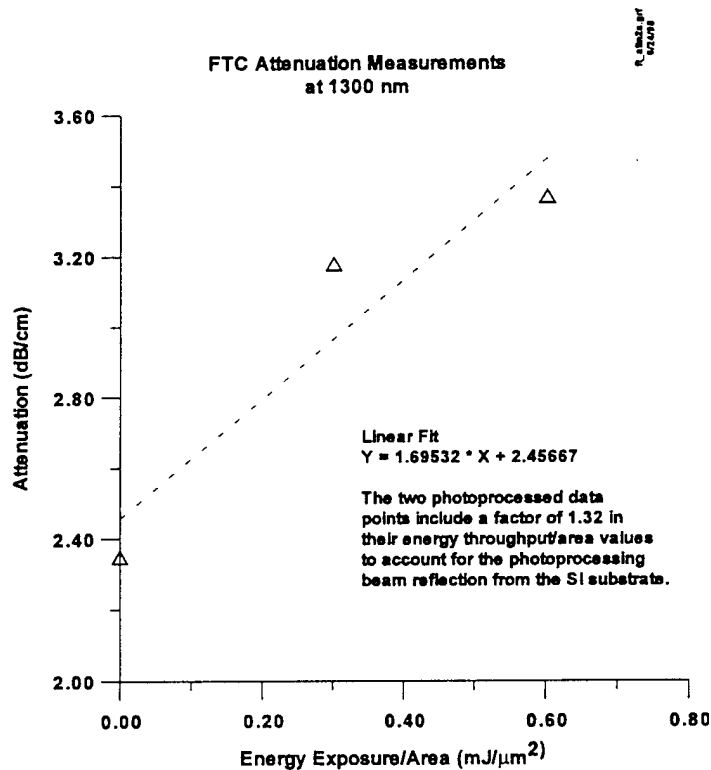


**Figure 28.** Attenuation in FTC.

#### 3.3.4.1.4 Transmittance

As mentioned in the discussion of APII, the determination of the transmittance under photoprocessing is critical for waveguide design in a dye/polymer system. Measurements of transmittance were made by directing a laser beam at a film sample while measuring the power emerging through the substrate as a function of time, and the intensity of the beam was estimated from the beam power as described in Equation 23. As discussed in Section 2.1, graphs of  $T(0)$ ,  $T(\infty)$ , and  $dT(0)/dt$  can be obtained from these types of measurements. Using Equations 1-3 on pg. 3, the  $A$ ,  $B$ , and  $C$  parameters may then be determined. These parameters could then be used to calculate the photoprocessing kinetics of a given film.

Two groups of these measurements were made in FTC. One group consisted of transmittance measurements made at 532 nm and 630 nm in films with 30% chromophore density of FTC, which were 1.6  $\mu\text{m}$  thick. The other group consisted of these types of measurements in films with 16% chromophore density, which were 2.0  $\mu\text{m}$  thick. The measurements are plotted, along with their values at early times. Linear curvefits in the early-time plots yield values of  $dT(0)/dt$ . The full-time plots yield estimates for  $T(0)$  and  $T(\infty)$ .

For the films with 30% chromophore density and 1.6  $\mu\text{m}$  thickness, Figures 29 and 30 show the long-time and early-time transmittances, respectively, for photoprocessing at 532 nm. Figures 31 and 32 show the long-time and early-time transmittances, respectively, for photoprocessing at 630 nm.

For the films with 16% chromophore density and 2.0  $\mu\text{m}$  thickness, Figures 33 and 34 show the long-time and early-time transmittances, respectively, for photoprocessing at 532 nm. Figures 35 and 36 show the long-time and early-time transmittances, respectively, for photoprocessing at 630 nm.

Values for the  $A$  and  $B$  parameters obtained from this data are listed in Table 2. Using these values for  $A$  and  $B$ , and estimating values of  $dT(0)/dt$  from curvefits in the early-time transmittance data, values of the  $C$  parameter have been calculated and plotted in Figure 37 for the 30% chromophore density, 1.6  $\mu\text{m}$  thick film, and in Figure 38 for the 16% chromophore density, 2.0  $\mu\text{m}$  thick film.

Having obtained the  $ABC$  parameters, it is then possible to calculate concentration profiles, and hence refractive index profiles, in dye/polymer films. Calculation of the concentration profiles is discussed in Section 2.

Some features of these results will be discussed in Sections 3.3 and 4.

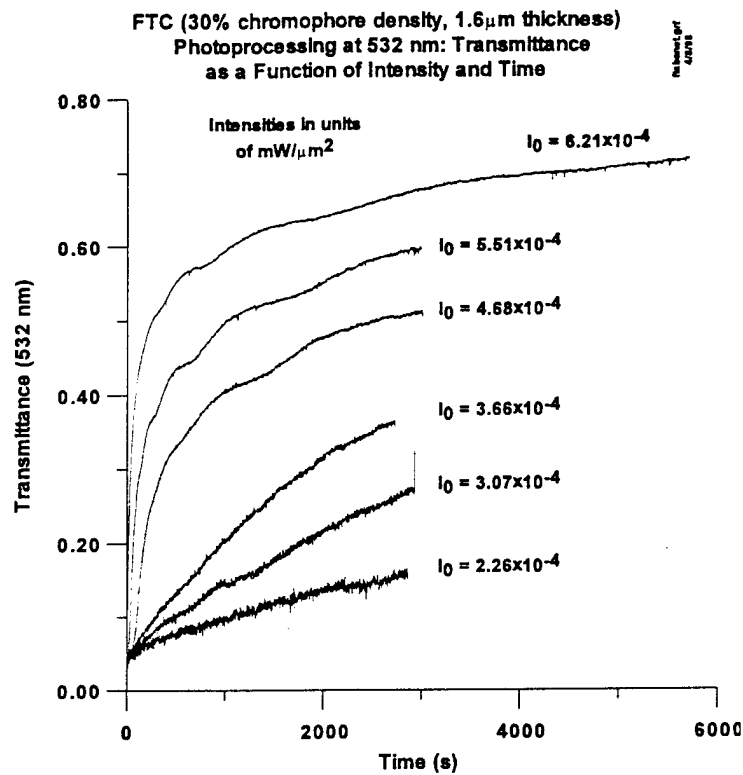


Figure 29. FTC Transmittance (Long-Time).

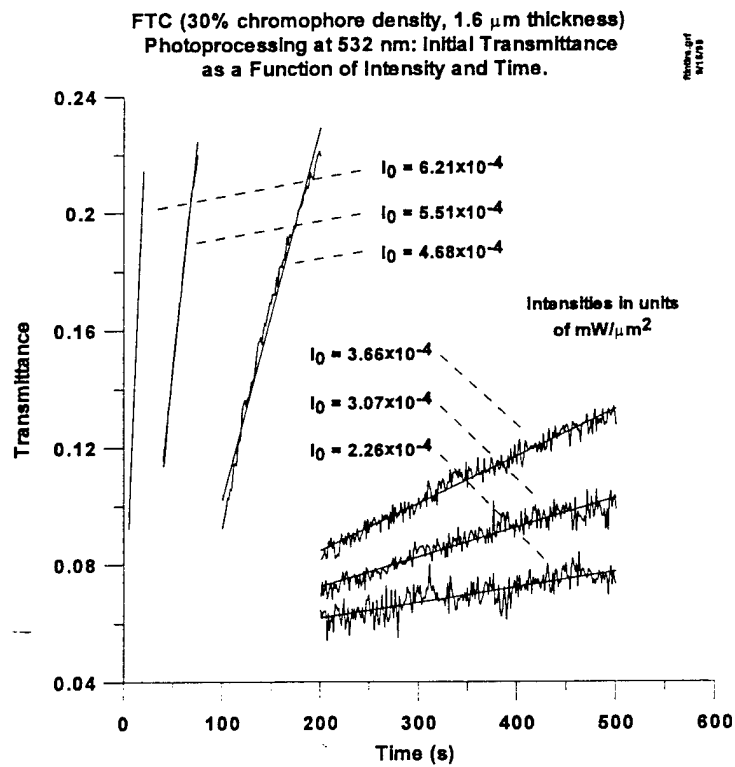


Figure 30. FTC Transmittance (Early-Time).

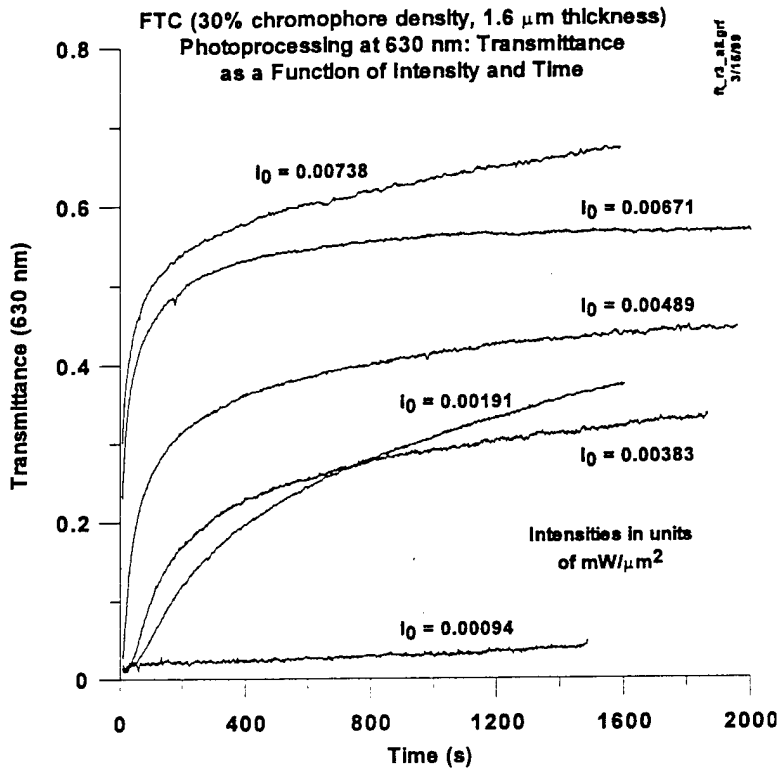


Figure 31. FTC Transmittance (Long-Time).

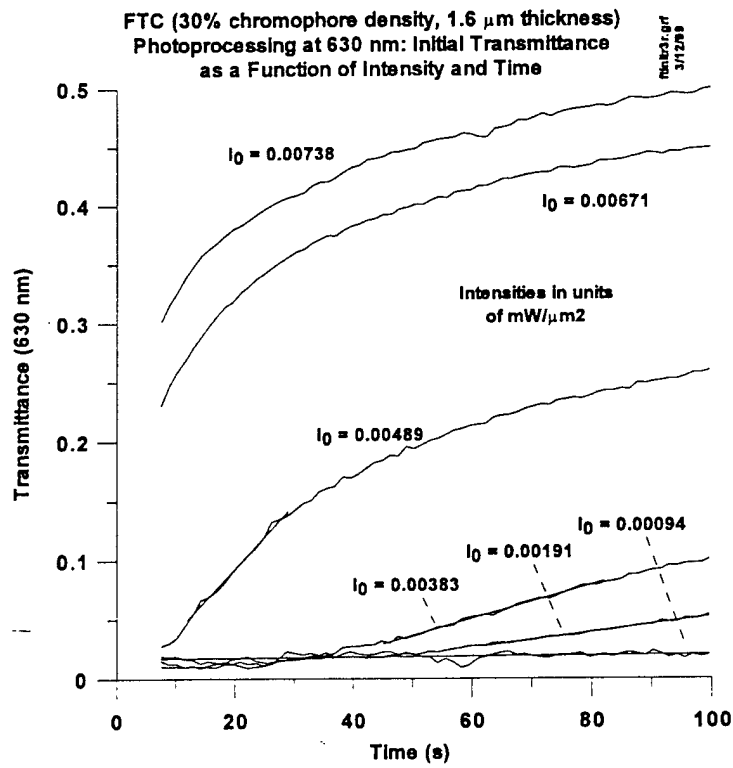


Figure 32. FTC Transmittance (Early-Time).

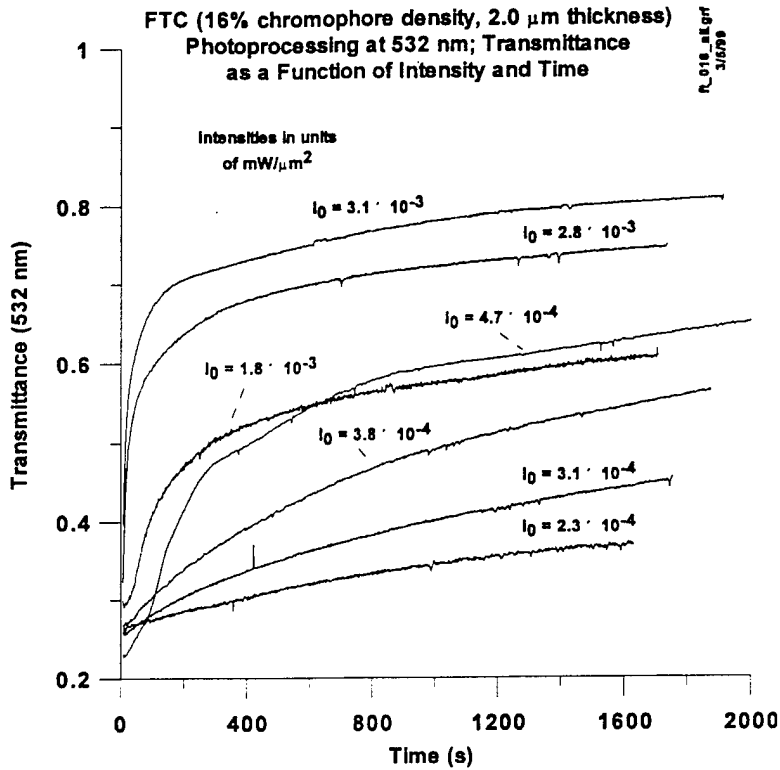


Figure 33. FTC Transmittance (Long-Time).

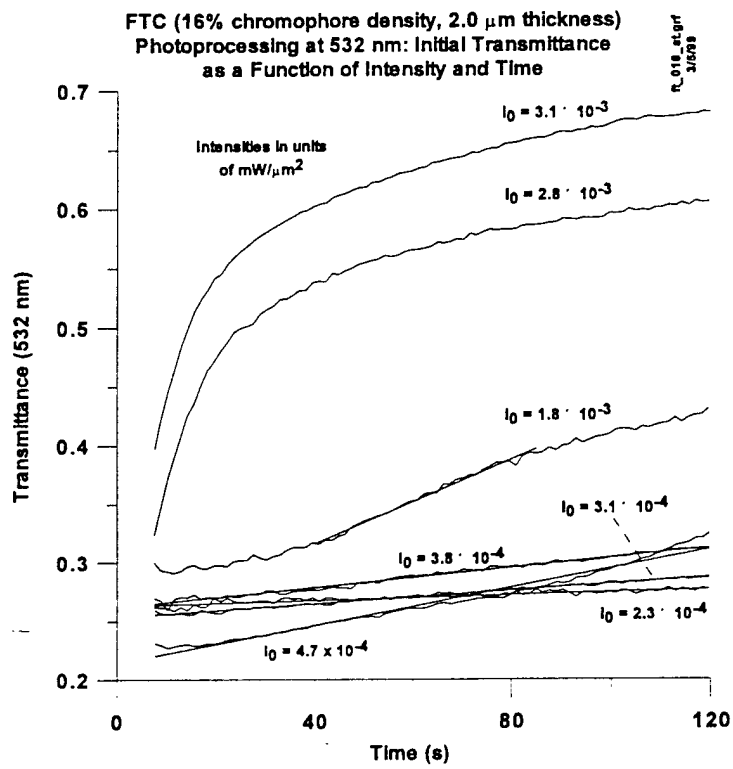


Figure 34. FTC Transmittance (Early-Time).

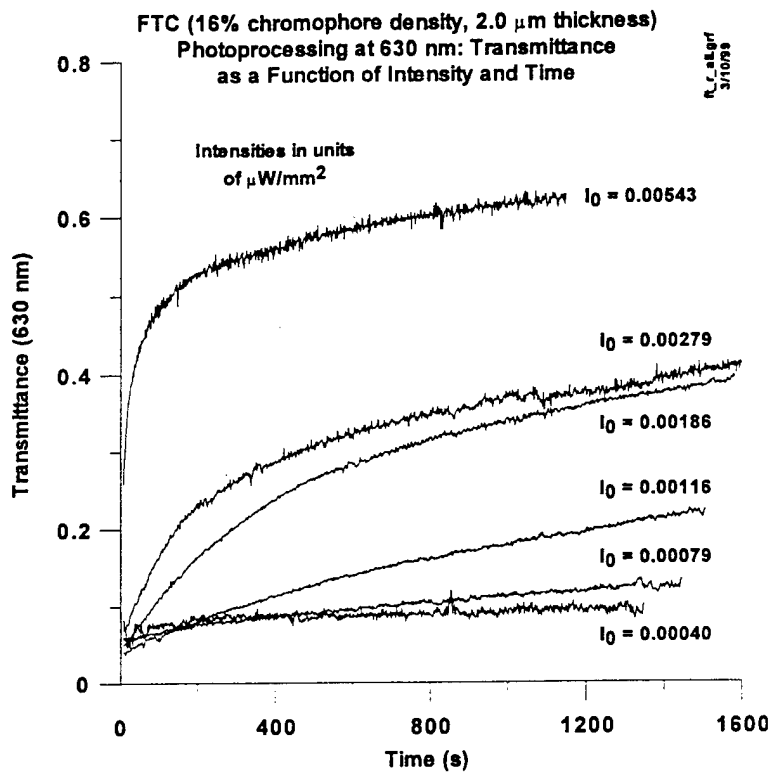


Figure 35. FTC Transmittance (Long-Time).

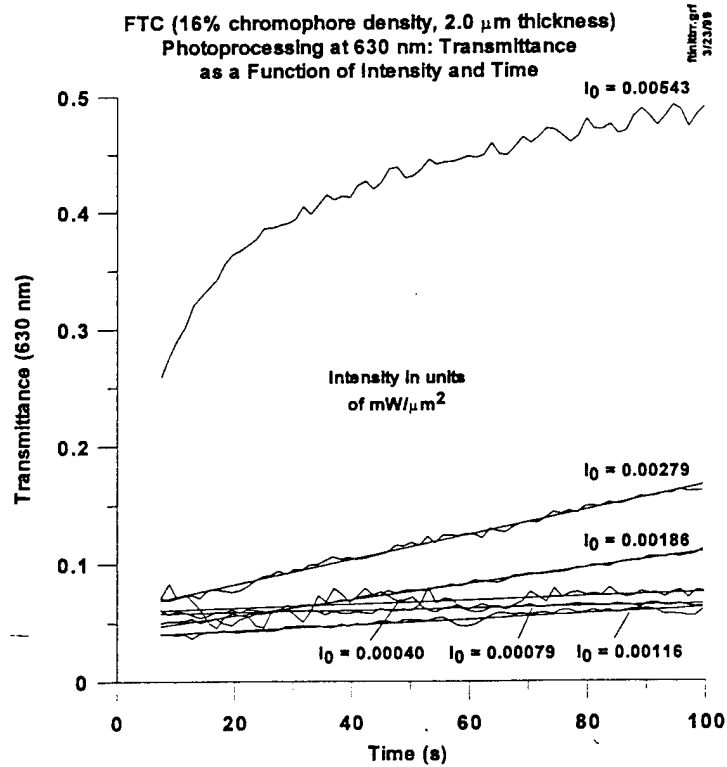


Figure 36. FTC Transmittance (Early-Time).

Film Parameters	Photoprocessing Wavelength	<i>A</i>	<i>B</i>
30% chromophore density 1.6 $\mu\text{m}$ thickness	532 nm	1.62	0.167
	630 nm	1.97	0.223
16% chromophore density 2.0 $\mu\text{m}$ thickness	532 nm	0.664	0.0932
	630 nm	1.29	0.208

Table 2. Values for the *A* and *B* Parameters

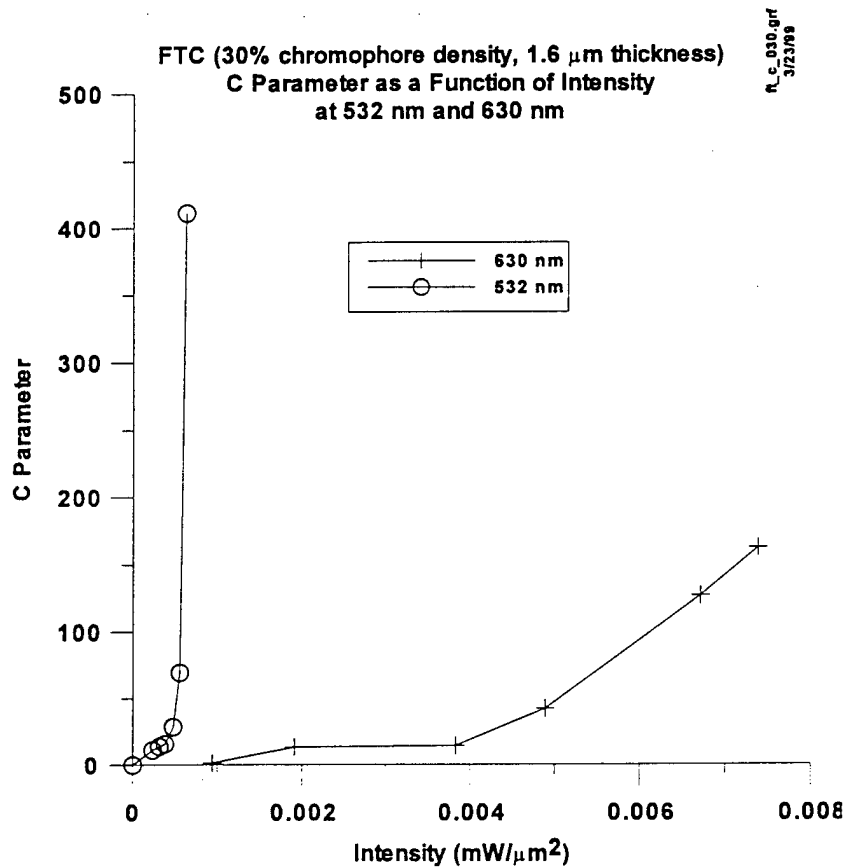


Figure 37. FTC C Parameters.

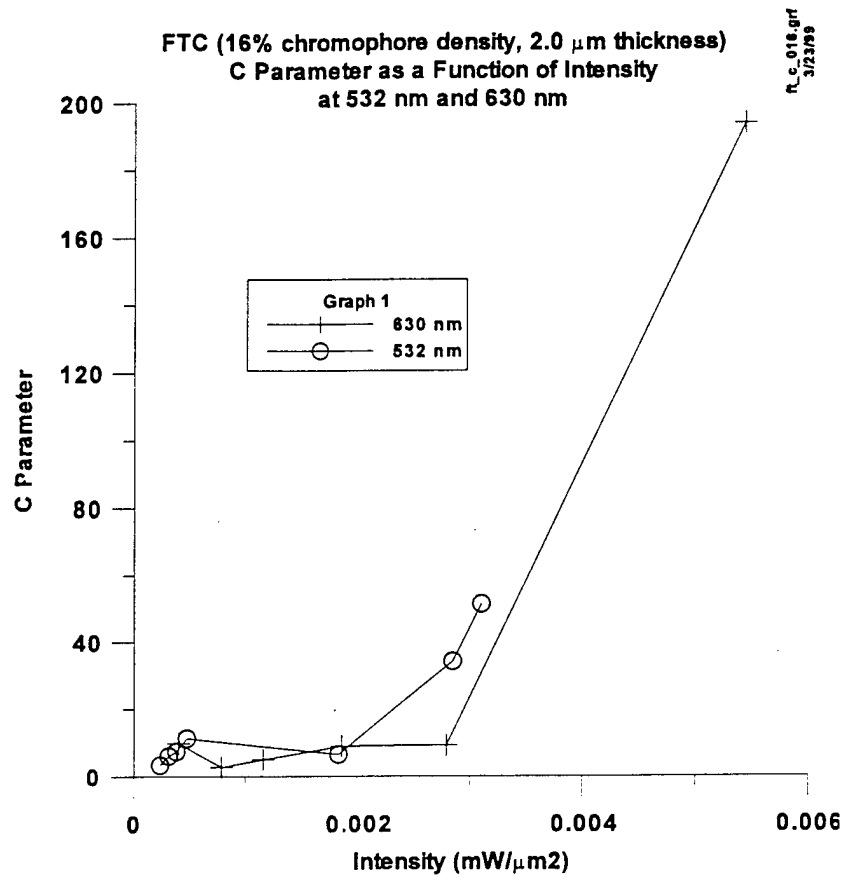


Figure 38. FTC C Parameters.

### 3.3 Photolithography of Channel Waveguides

Buried channel waveguides in FTC have been prepared by heavy photoprocessing a thick (8  $\mu\text{m}$ ) film (16% chromophore) sample through a patterned mask placed over the film, then removing the mask and lightly rephotoprocessing the same area. The mask consisted of an aluminum film on a glass substrate (Figure 39). It was made using standard semiconductor manufacturing lithographic techniques, and included channel patterns of varying widths and lengths.

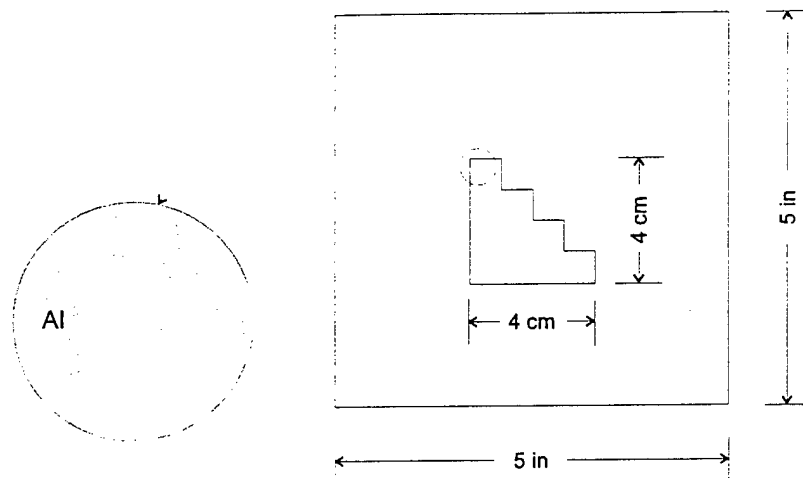


Figure 39. Mask for Photoprocessing.

The photoprocessing procedure was similar to that used in patterning positive photoresist. The mask was placed over an unphotoprocessed 8  $\mu\text{m}$ -thick FTC film, and the mask/film assembly was stepped, using the MM2000 Positioner, under a 532 nm beam from the diode laser. The photoprocessing was intense enough to largely eliminate the chromophore from the film under the transparent areas of the mask. This step left high-refractive-index regions from the substrate to the surface of the film that constituted multimode 1300 nm channels. These channels were roughly rectangular in cross-section, with dimensions of about 8  $\mu\text{m}$   $\times$  10  $\mu\text{m}$ .

A set of attenuation measurements were made on a set of these channels. The channels were cleaved to give clean ends perpendicular to the film surface, and were then endfired with 1300 nm light through a single-mode optical fiber. The emitted radiation was captured by a multimode fiber and directed to a detector, as shown in Figure 40. By shortening the channels with additional cleaves, a set of attenuation measurements were made of beam attenuation in the channels as a function of length. These results are shown in Figure 41, and indicate an attenuation coefficient for multimode 1300-nm radiation in the film of about 6.9 dB/cm, as obtained from the curvefit shown in this Figure.

These results show an approximate 4 dB/cm increase in loss with waveguiding compared to the planar FTC films that were analyzed (Figure 28). Additional attenuation studies were not undertaken with these waveguides since the waveguides were unoptimized and intended for

demonstrating direct photoprocessing of buried waveguides in NLO films. From the intercept in Figure 41, the coupling losses are estimated to be about 0.9 dB/endface. This is reasonable considering the unpolished waveguide edges and unmatched refractive index differences between the NLO polymer and the fiber.

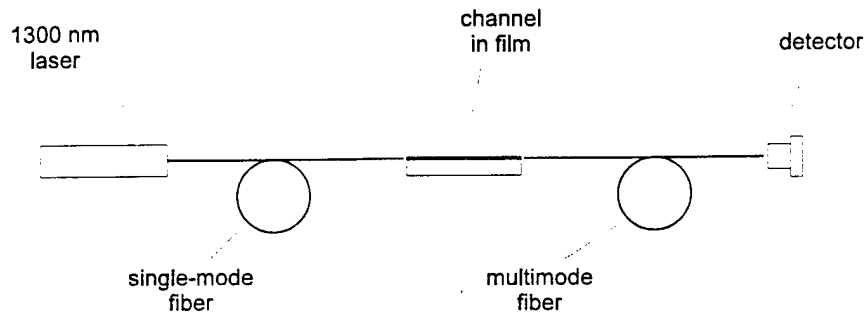


Figure 40. Endfiring Channels With Optical Fibers.

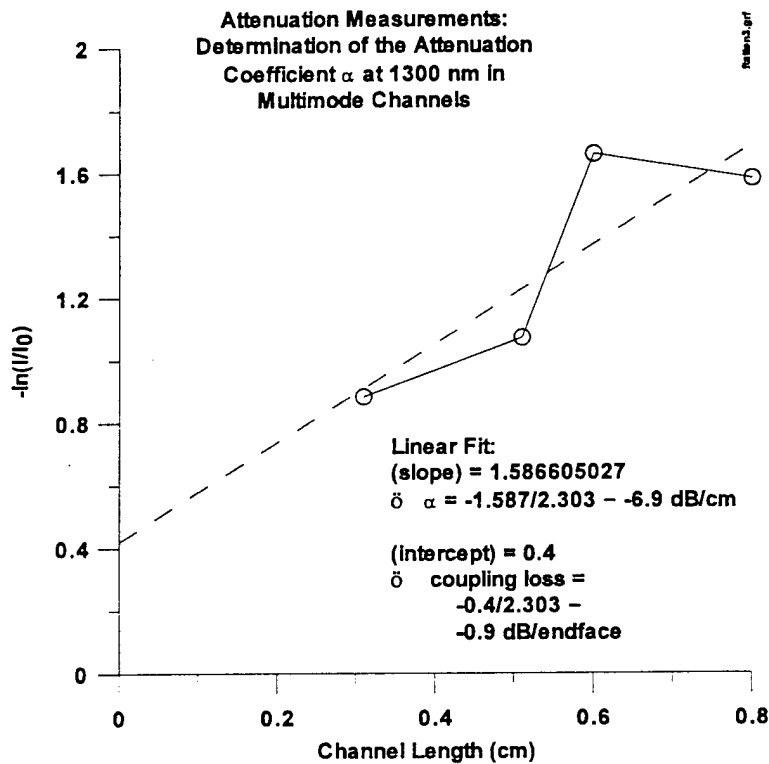
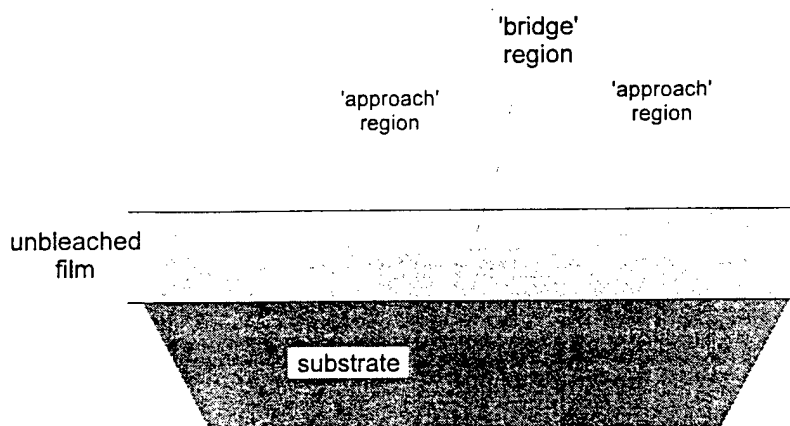


Figure 41. Attenuation in FTC Multimode Channels.

Additional sets of channels were then photoprocessed in the film using the above procedure. To bury the channels, they were then subjected to a second photoprocessing without the mask<sup>1</sup>. The intensities for this photoprocessing were varied over the channel region to remove chromophore material near the surface, as shown in Figure 42. The 'bridge' in this pattern constitutes the buried channel region. The 'approaches' are designed to allow continuous mode matching between the channel faces, which might interface with optical fibers, to the smaller modes allowed in the buried 'bridge' region (see the discussion on pg. 2).



**Figure 42.** Cross-Section of a 'Bridge' Photoprocessed Through a Buried Channel.

Three sets of buried channels were photoprocessed into the film. A photomicrograph of the approach region of one of them as viewed from the top is shown in Figure 43. It should be noted that the third and fourth channels from the right in this image are double channels.

---

<sup>1</sup>The second photoprocessing was again done at 532 nm. Ideally, this photoprocessing would have been done at a wavelength under the absorption band to get enhanced photoprocessing nearer the film surface, but limitations of the dye laser precluded this.

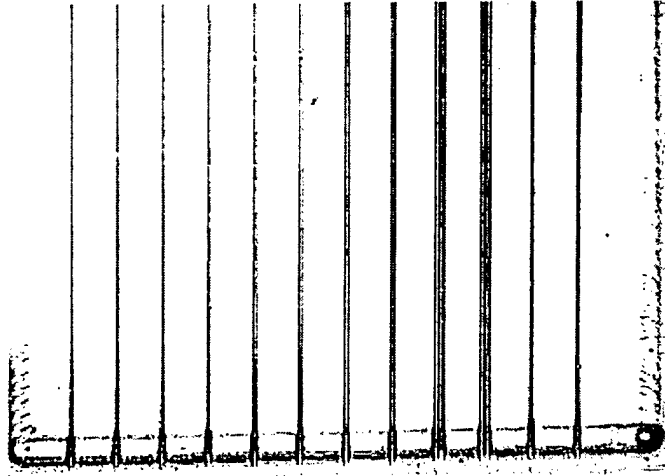
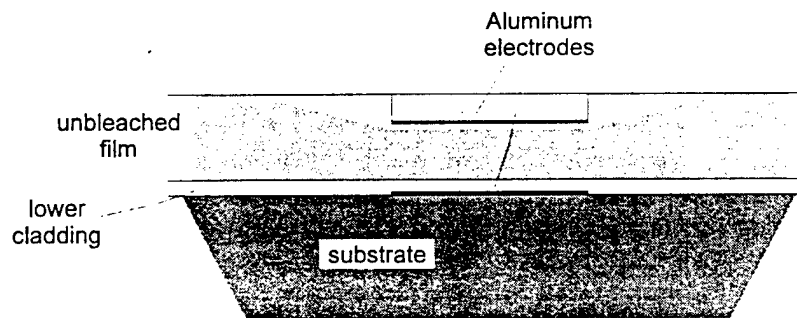


**Figure 43.** 10  $\mu\text{m}$ -Wide Channels in an 8  $\mu\text{m}$  Thick FTC Film.

The surface of the film was then etched away over the 'bridge' region in the channel sets. The material was removed to a depth of about 2  $\mu\text{m}$  using reactive ion etching (RIE). This was to demonstrate that material can be removed from above buried channels, and that high-frequency, low-drive-voltage electrodes can be optimally deposited just above the buried channel regions. Such a design is illustrated in Figure 44.



final\_11.cdr

**Figure 44.** Etched Waveguide with Cladding and Electrodes.

An image of the region between an 'approach' region and the 'bridge' region for a channel set is shown in Figure 45. The etched region is at the top of the Figure. It may be seen that, although a substantial amount of material has been removed, the channels are still clearly present<sup>2</sup>.

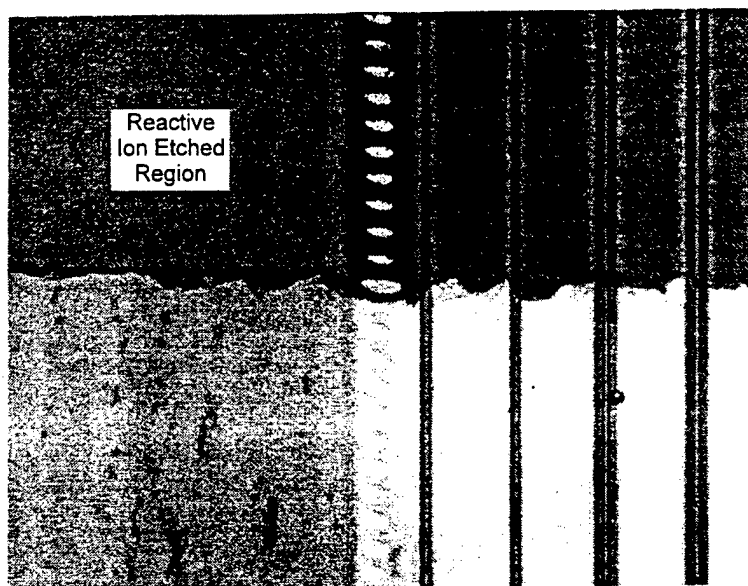


**Figure 45.** Etched Region Adjoining an Unetched Region in a Channel Set.

These results demonstrate the capability of applying waveguide photoprocessing using lithographic techniques in combination with RIE to create buried waveguide structures in films whose thickness can be varied. By using a lower electrode, a cladding layer, and then depositing an upper electrode as shown in Figure 44, larger waveguides can be made which taper to small ones between closely spaced electrodes for reduced drive voltages. By selecting photoprocessing wavelengths together with appropriate NLO materials, waveguide structures can be made which lack birefringence, are stable, and are insensitive environmental temperature and optical irradiation. Both the APII and FTC NLO materials developed by USC appear to provide these features for advanced waveguide structure development.

---

<sup>2</sup>The rough boundary edge for the RIE region is the result of the masking used for the RIE process. Also, faint horizontal striations in the polymer film between waveguides are observable. These may be residual ripple in the photoprocessing which is visible in the thinner, contrast-viewed, etched region of the film.